FERMILAB-PUB-09-124-E

SEARCHES FOR THE STANDARD MODEL HIGGS BOSON AT THE CDF EXPERIMENT

SONG-MING WANG
Institute of Physics, Academia Sinica, No. 128, Sec. 2, Academia Rd., Nangang, Taipei City 11529, Taiwan.
smwang@phys.sinica.edu.tw

The understanding of the dynamics behind the breaking of the electroweak symmetry is one of the most important goals in the field of high energy physics. In the standard model (SM) the Higgs mechanism plays a key role in the symmetry breaking, one manifestation of which is spin-0 Higgs boson. Thus the search for the Higgs boson is one of the flagship analyses at the Tevatron. Over the past few years the CDF experiment has made significant improvements in its sensitivity on the search for the SM Higgs boson. In this paper we summarize CDF's most recent results on the searches for the SM Higgs boson production at the Tevatron using data samples of integrated luminosities up to 3 fb^{-1}. We also present the Tevatron's latest combined results on the SM Higgs boson search, and discuss the possibility that it could be found at the Tevatron in the near future.

Keywords: Higgs; Tevatron; CDF; DZero.

PACS numbers: 14.80.Bn

1. Introduction

The standard model appears to be close to complete experimental verification after the discoveries of the Top quark at the Tevatron in 1995 [1] and the tau neutrino in 2000 [2], representing its final fermionic pieces. The last particle predicted by the SM, which has not yet been observed in experiments, is the Higgs boson. In the SM the electromagnetic and weak interactions are unified under the $\mathrm{SU(2)_L \times U(1)_Y}$ gauge symmetry. The gauge invariance of the theory requires the vector bosons to be massless. However, experimentally we know that the $W^{\pm}$ and Z^0 vector bosons have non-zero masses. Therefore the electroweak symmetry has to be broken. In the SM, the breaking is achieved through the Higgs mechanism, which postulates the existence of a Higgs field that permeates the entire universe. The Higgs field is a complex doublet of scalar fields that has two neutral and two charged components. The electroweak symmetry is spontaneously broken when the Higgs fields acquires a non-zero vacuum expectation value. The $W^{\pm}$ and Z^0 bosons obtain their masses by, respectively, absorbing the two charged components and one of the two neutral component scalar fields. The remaining neutral component of the complex doublet is an elementary physical scalar state whose mass is not predicted at tree level by the SM; the Higgs boson. The masses of the fermions are generated when the fermions couple to the Higgs boson via Yukawa interactions. The strength of the Yukawa couplings are proportional to the masses of the fermions.

As mentioned earlier the Higgs boson's mass at tree level is not predicted in the SM. The theoretical bounds from vacuum stability and unitary constraints requires the Higgs boson mass to be in a specific range for a given value of Λ, which is the scale that new physics beyond the SM must enter. This boundary on the Higgs mass as a function of Λ is shown in Fig. 1 [3].

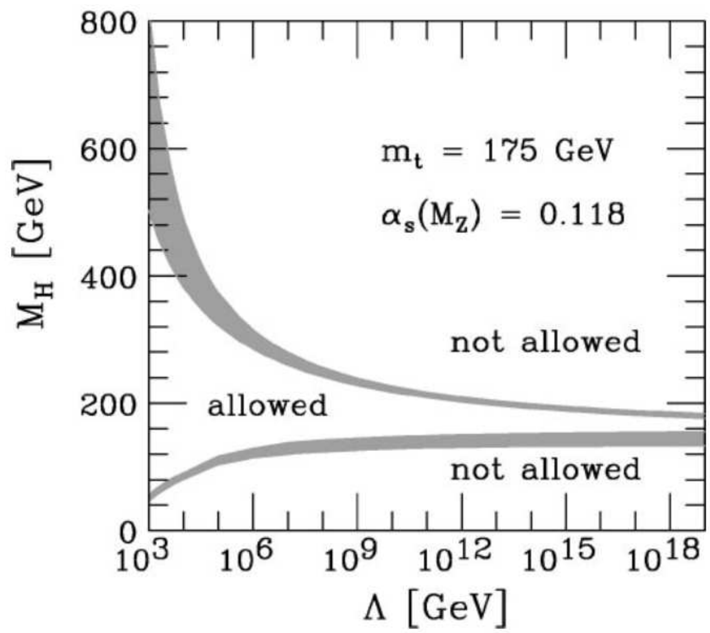

Fig. 1. The lower and upper bounds of the Higgs mass as a function of the energy scale Λ at which new physics beyond the SM must enter.

Higher order loop diagrams, such as those illustrated in Fig. 2, will introduce a quadratic divergent correction to the Higgs mass of the order

$$\Delta m^2 \sim \frac{\Lambda^2}{16\pi^2}. \tag{1}$$

The correction can be very large if Λ is near the Planck scale ($\sim 10^{19}$ GeV). Fig. 1 implies that the Higgs mass is required to be smaller than 1 TeV, which means that the bare mass of the Higgs boson must be fine-tuned to a precision of over 16 orders of magnitude to yield a Higgs mass of the order of a TeV. This fine-tuning problem (also known as the hierarchy problem) appears to make the SM very un-natural.

The Higgs mechanism in the SM provides a framework to explain the observed masses of the gauge bosons (W and Z) and the fermions, however, the fundamental dynamics of the electroweak symmetry breaking are not known. The fine-tuning

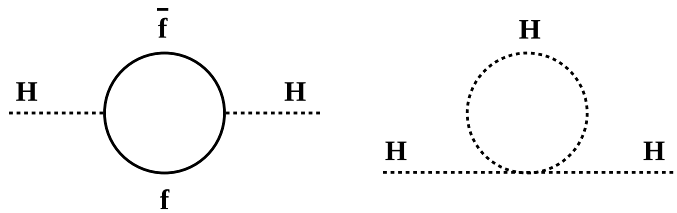

Fig. 2. Diagrams of higher order corrections to the Higgs boson mass.

of the Higgs mass also creates an un-naturalness problem to the SM. Therefore, a theory beyond the SM is required to provide a fundamental explanation to the mechanism behind the electroweak symmetry breaking and to solve the naturalness problem.

1.1. *Direct Searches for the Standard Model Higgs Boson at Non-Tevatron Experiments*

Several experiments have performed direct searches for the SM Higgs boson over the last couple of decades. Before the LEP (Large Electron Positron) collider began its operation in 1989, light Higgs boson masses below 5 GeV/c^2 were excluded by experiments [4] that searched for Higgs boson production via W bosons in pion decays ($\pi^+ \to W^{+*} \to e^+\nu_e H$), or via flavor-changing neutral current decays ($K_L^0 \to \pi^0 H$, $B \to K^0 H$). During the LEP1 operation phase (1989-1995) the machine was running at the center-of-mass (CM) energy close to the Z boson resonance. The energy gradually increased to 209 GeV during the LEP2 phase of operation. At LEP the Higgs boson is expected to be produced mainly through the Higgsstrahlung process $e^+e^- \to HZ$. The Higgs boson can also be produced from the fusion of a pair of W or Z bosons. However, their production cross section is much smaller than the Higgsstrahlung process. The predicted total Higgs boson production cross section is in the order of $\sim$ 1 pb for $m_H < E_{\rm CM} - M_Z$, where $E_{\rm CM}$ is the center-of-mass energy. For the case where $m_H > E_{\rm CM} - M_Z$, the predicted cross section is about a magnitude smaller. The four experiments at LEP (ALEPH, DELPHI, L3 and OPAL) searched for the Higgs boson [5,6,7,8] through the Higgsstrahlung production process, with the following decay channels considered :

- $H \to b\bar{b}$, $Z \to l^+l^-, \nu\bar{\nu}, q\bar{q}$ ($l = e$, μ or τ)
- $H \to \tau^+\tau^-$, $Z \to q\bar{q}$

The total integrated luminosity of the combined e^+e^- collision data from the four experiments was 2461 pb^{-1} for center-of-mass energies ranging from 189 to 209 GeV. In the LEP2 data ALEPH reported an excess of three standard deviations, indicating the possible production of a SM Higgs boson at a mass of 115 GeV/c^2. However, the data from the other three experiments did not show evidence for such an excess. The search results from all four experiments were combined and set a lower bound on the Higgs boson mass of 114.4 GeV/c^2 at 95% C.L. [9]. If no Higgs boson signal is present, the expected lower bound on the Higgs boson mass is 115.3 GeV/c^2. The observed and expected limit on the Higgs boson mass is shown in Fig. 3.

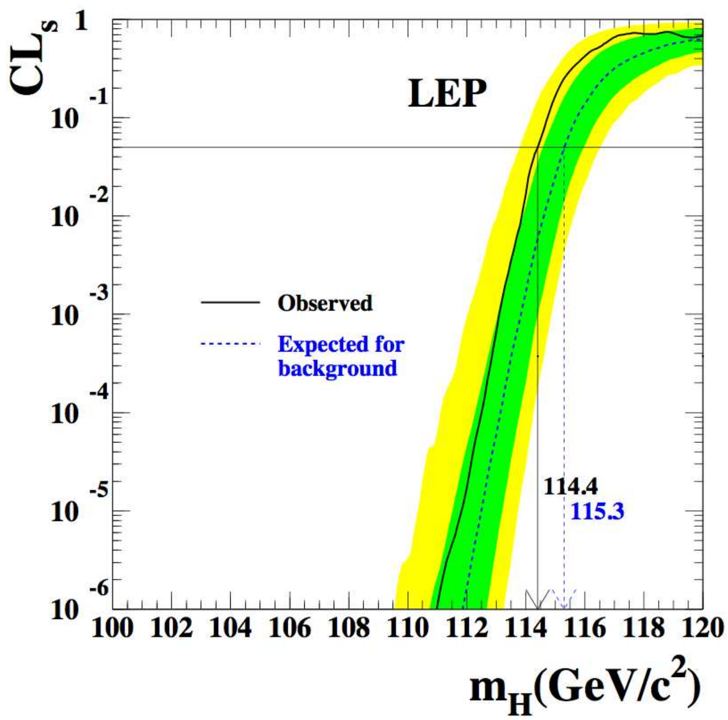

Fig. 3. The ratio $CL_s = CL_{s+b}/CL_b$ for the signal plus background hypothesis as a function of the test Higgs mass m_H. CL_b is the compatibility of the observation with the background hypothesis, whereas CL_{s+b} is the compatibility of the observation with the signal plus background hypothesis. The observed 95% C.L. lower bound on the mass of the SM Higgs boson is obtained from the intersection of the horizontal line for $CL_s = 0.05$ with the observed curve.

1.2. *Indirect Constraint on the Higgs Boson Mass*

Although the Higgs boson has not yet been observed in experiments, its mass may be inferred indirectly from fits to precision measurements of electroweak observables. For example, the masses of the W and Z bosons receive radiative corrections in the form of loop diagrams. Examples of such loop diagrams involving the W boson are shown in Fig. 4 where the loop corrections to the W mass receive contributions from the Higgs boson and the Top quark. Thus, the W boson mass is sensitive to both the masses of the Higgs boson and the Top quark. Similarly due to the contribution of the Higgs boson in the Z boson mass correction loop, the Z boson mass is also sensitive to the Higgs boson mass. The mass $m_H = 84^{+34}_{-26}$ GeV/c^2 is obtained from a global fit to the precision electroweak data accumulated at LEP, SLC, the Tevatron and elsewhere [10]. The 95% C.L. upper limit on the Higgs mass obtained from the fit is 154 GeV/c^2. If the limit $m_H = 114.4$ GeV/c^2 from LEP's direct search is taken into account, the adjusted 95% C.L. upper limit will be $m_H < 185$ GeV/c^2.

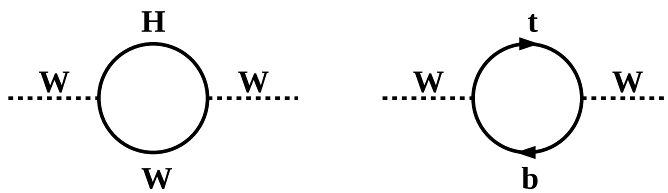

Fig. 4. Loop corrections to the W boson mass.

2. Higgs Boson Production and Decay Channels

2.1. *Production of the Standard Model Higgs Boson at the Tevatron*

At the Tevatron the Higgs boson can be produced in $p - \bar{p}$ interactions through several processes [11]. The production cross section of these processes as a function of the Higgs boson mass is shown in Fig. 5. The cross section values in the figure are taken from [12]. The most dominant production processes are:

- $gg \to H$, where the Higgs boson is produced via the fusion of a pair of gluons. The fusion happens primarily through a Top quark loop since the Top quark is the heaviest quark. The production cross section varies between 1 pb and 0.2 pb for Higgs boson masses between 100 and 200 GeV/c^2.
- $q\bar{q}' \to WH/ZH$, where the Higgs boson is produced in association with a vector boson (W or Z). The production cross section is about 0.5 pb for a Higgs boson mass of 100 GeV/c^2, and about 0.03 pb for a mass of 200 GeV/c^2.
- $qq \to qqH$. In this process each of the incoming quarks of the colliding proton and anti-proton, radiates a vector boson (W or Z) which then annihilate to produce a Higgs boson. The process is known as vector boson fusion. The production cross section varies between 0.1 pb to 0.02 pb for Higgs boson masses between 100 to 200 GeV/c^2.

The Feynman diagrams of these three most dominant production processes are shown in Fig. 6.

The other SM Higgs production processes at the Tevatron are the associated production of a Higgs boson and a heavy-flavor quark pair ($gg, q\bar{q} \to Hb\bar{b}$, $gg, q\bar{q} \to Ht\bar{t}$), and the Higgs production via the fusion of a pair of b-quarks ($b\bar{b} \to H$). These production processes have much smaller cross section (~ 0.1 fb $-$ 0.1 pb) and have very small sensitivity in the Higgs search.

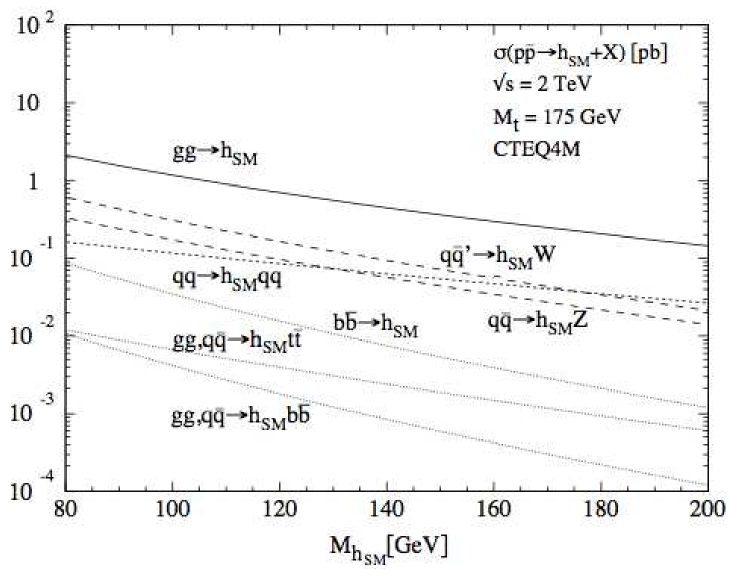

Fig. 5. Higgs boson production cross sections for various production channels at the Tevatron as a function of the Higgs mass.

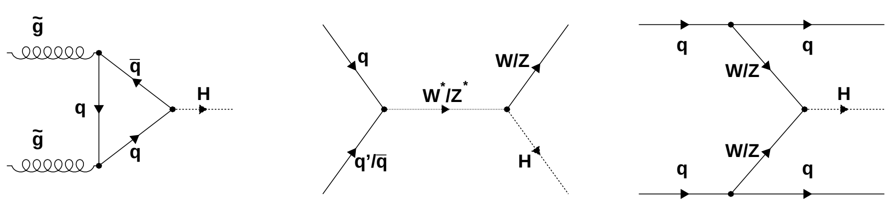

Fig. 6. Feynman diagrams of the three most dominant SM Higgs boson production processes at the Tevatron. (Left) Higgs boson produced via the fusion of a pair of gluons. (Middle) Higgs boson produced in association with a vector boson. (Right) Higgs boson produced via the vector boson fusion process.

2.2. *Decays of the Higgs Boson*

The branching ratios of the Higgs boson decay vary as a function of the Higgs mass. This dependence is shown in Fig. 7. The branching ratios are obtained with the program HDECAY [13]. For the Higgs boson mass below $\sim$ 135 GeV/c^2 the dominant decay channel is $H \to b\bar{b}$. The branching ratio of this channel at a Higgs mass of 100 GeV/c^2 is $\sim$ 80%. The second most dominant decay channel for low Higgs mass is $H \to \tau^+\tau^-$, with a decay branching ratio of $\sim$ 10% for a Higgs mass of $m_H <$ 110 GeV/c^2. For the Higgs boson mass above $\sim$ 135 GeV/c^2 the decay channel $H \to W^+W^-$ becomes the dominant decay channel, where one of the W boson is necessarily off-shell if $m_H <$ 160 GeV/c^2.

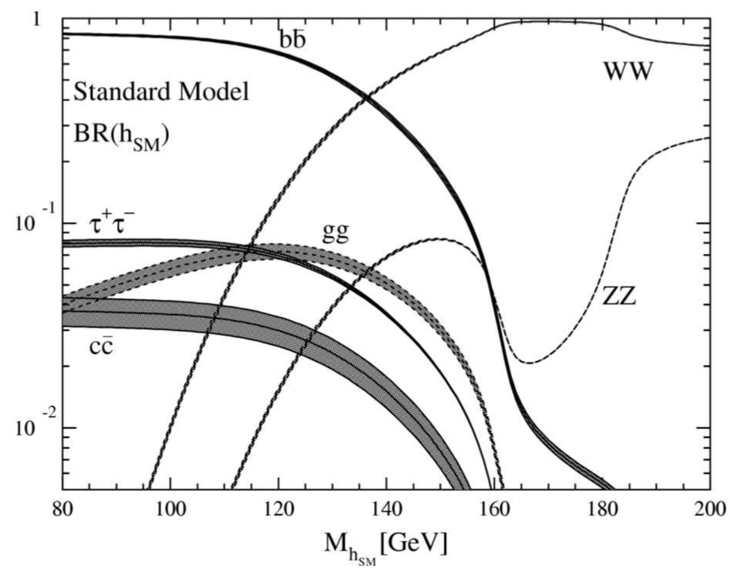

Fig. 7. The Higgs boson decay branching ratios for various decay channels as function of the Higgs mass.

3. Accelerator and Detector

3.1. *The Tevatron*

The Tevatron is a proton-antiproton collider located at the Fermi National Accelerator Laboratory, in Batavia, Illinois. The center-of-mass energy during the Run II operation is 1.96 TeV. At the Tevatron the proton bunches and anti-proton bunches cross each other every 396 ns. The designed highest instantaneous luminosity is $L = 3 \times 10^{32}\text{cm}^{-2}\text{s}^{-1}$. The collider started its Run II operation in the summer of 2001. Since then and up to now (summer 2008) it has delivered a total integrated luminosity of $\sim$ 5 fb^{-1} to each of the CDF and DØ experiments, and each experiment has collected about $\sim$ 4 fb^{-1}. The machine has also reached and surpassed its designed peak instantaneous luminosity. A detailed description on the Tevatron can be found in Ref. 14.

3.2. *The CDF II Detector and Data Reconstruction*

CDF II is a general-purpose detector that consists of several sub-detector components. Here we provide a brief description of the detector, whereas a detailed description can be found elsewhere [15]. The charged-particle tracking system is closest to the beam pipe, and consists of multiple layers of silicon micro-strip detectors, which cover a pseudorapidity region $|\eta| < 2$, and a large open-cell drift chamber covering the pseudorapidity region $|\eta| < 1$ [16,17]. The definition of pseudorapidity is given in Ref. 18. The silicon microstrips of the silicon detectors have a pitch of 25 to 65 μm, depending on the layer, allowing a precise measurement of a track's impact parameter with respect to the primary vertex. The tracking system is enclosed in a superconducting solenoid, which in turn is surrounded by calorimeters. The calorimeter system [19] is organized into electromagnetic (EM) and hadronic (HAD) sections segmented in projective tower geometry, and covers the region $|\eta| < 3.6$. The electromagnetic calorimeters use lead-scintillator sampling, whereas the hadron calorimeters use an iron-scintillator sampling technique. The transverse energy resolution of the electromagnetic calorimeters is $\sigma(E_T)/E_T = \frac{13.5\%}{\sqrt{E_T(\mathrm{GeV})}} \oplus 2\%$ for the central region ($|\eta| < 1$), and $\sigma(E)/E = \frac{16\%}{\sqrt{E}(\mathrm{GeV})} \oplus 1\%$ for the forward region ($|\eta| > 1$). The transverse energy resolution of the hadronic calorimeters is $\sigma(E_T)/E_T = \frac{75\%}{\sqrt{E_T(\mathrm{GeV})}} \oplus 3\%$ for the central region, and $\sigma(E)/E = \frac{80\%}{\sqrt{E}(\mathrm{GeV})} \oplus 5\%$ for the forward region. Shower maximum detectors embedded in the electromagnetic calorimeters at approximately six radiation lengths help in the position measurement and background suppression for electrons and photons. Outside the central calorimeters are scintillators and drift chambers for identifying muons as minimum ionizing particles.

The $p\bar{p}$ interactions recorded by the CDF detector have to satisfy three levels of online event selection. The selected events are then processed offline to construct physics objects to be used in the analyses. In the offline system an electron candidate is identified as a track associated with a cluster in the electromagnetic calorimeter [20]. Its electromagnetic to hadronic energy ratio and shower profile, must also be consistent with that expected for electrons. Electrons can be identified up to a pseudorapidity range $|\eta| < 2.8$. Candidate muons are identified as tracks that extrapolate to hits in the muon chambers and to energy deposited in the calorimeters consistent with a minimum ionizing particle [20]. The pseudorapidity range for identifying muons is up to $|\eta| < 1$. To increase lepton detection efficiency, candidate leptons (electrons, muons, taus) may also be identified by isolated tracks with momentum above a certain threshold, to be used in some analyses.

Jets are reconstructed from energy deposits in calorimeter towers using a cone algorithm with fixed radius $\Delta R \equiv \sqrt{\Delta\eta^2 + \Delta\phi^2}$ in $\eta - \phi$ space [21]. For the analyses discussed later in this article a cone size of 0.4 is used. Corrections are applied to account for effects that can cause mismeasurements in the jet energy such as non-linear calorimeter response and multiple beam interactions. The measured jet energy is also corrected back to the particle or parton level [22]. The missing transverse energy is defined as the energy imbalance in the plane transverse to the beam direction. The missing transverse energy vector, $\vec{\not\!\!E}_T$, is $-\sum_i E_T^i \mathbf{n_i}$, where $\mathbf{n_i}$ is the unit vector in the azimuthal plane that points from the beamline to the i^{th} calorimeter tower. The scalar quantity $\not\!\!E_T$ is the magnitude of the vector $\vec{\not\!\!E}_T$. Both magnitude and direction of $\vec{\not\!\!E}_T$ are recomputed after the jet energies are corrected and for muons which do not deposit all of their energy in the calorimeter.

At CDF b jets are identified via either of several b-tagging algorithms. The two most common algorithms employed in the SM Higgs boson searches are the SECVTX and the JET-PROBABILITY. The SECVTX algorithm [23] looks for tracks within jets that form a secondary vertex significantly displaced from the primary interaction point. The JET-PROBABILITY algorithm [24] examines the impact parameter of the tracks within a jet and computes a probability that the jet is a b jet. Jets from b partons are characterized by secondary decays that are displaced from the primary vertex; thus their tracks have a large impact parameter. Light-flavor jets appear to come from the primary interaction and their tracks' impact parameter are consistent with the primary vertex (within the resolution of the tracking detector). Both SECVTX and JET-PROBABILITY algorithms can tag a b jet using a tight selection criteria or a loose selection criteria. The performance of both algorithms are quite similar. The tight (loose) tagging efficiency for b jets is about $\sim 40\%$ ($\sim 50\%$) and the misidentification rate for light quarks (u, d, s) and gluon jets is $\sim 1\%$ ($\sim 2-5\%$).

4. Searches for the Standard Model Higgs Boson at CDF in Run I

The CDF experiment searched for the SM Higgs boson production in association with a vector boson (W or Z) on a data sample of 106 pb^{-1} collected during the Run I data taking period. At that time the Tevatron collided proton beam on anti-proton beam at $\sqrt{s} = 1.8$ TeV. The search for the Higgs boson was conducted in four separate channels based on Higgs bosons decaying into $b\bar{b}$ pairs. The channels were :

- $WH \to l^{\pm}\nu b\bar{b}$ ($l = e$ or μ)
- $WH/ZH \to q\bar{q}'b\bar{b}$
- $ZH \to l^+l^-b\bar{b}$
- $ZH \to \nu\bar{\nu}b\bar{b}$

The production cross sections of WH/ZH vary between 0.5 pb and 0.15 pb for Higgs boson masses between 90 and 130 GeV/c^2. No Higgs production signal was seen in any of the four search channels and their results were combined to set a 95% C.L. upper limits on $\sigma(p\bar{p} \to VH) \times \beta$, where β is the branching ratio of the Higgs boson decaying into $b\bar{b}$. For Higgs boson masses of 90, 110 and 130 GeV/c^2, the limits were 7.8, 7.2 and 6.6 pb respectively [25]. The results of these analyses are summarized in Fig. 8.

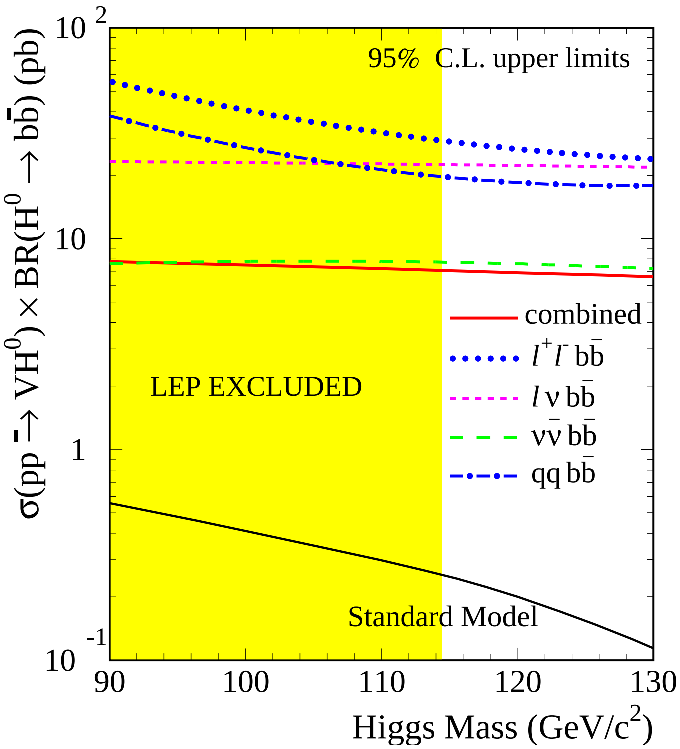

Fig. 8. The 95% C.L. upper limits on $\sigma(p\bar{p} \to VH) \times \beta$ of the SM Higgs boson searches at CDF in Run I. β is the branching ratio of the Higgs boson decaying into $b\bar{b}$.

5. Searches for the Standard Model Higgs Boson at CDF in Run II

The search for the SM Higgs boson at CDF in Run II can be categorized into low Higgs mass ($m_H \lesssim 135$ GeV/c^2) and high Higgs mass ($m_H \gtrsim 135$ GeV/c^2) searches. The production and decay channels considered by CDF are shown in Table 1. For both low and high Higgs mass searches, CDF has looked at the four highest predicted Higgs boson production rate processes at the Tevatron. In the case of the Higgs decay channels, the $H \to b\bar{b}$ and $H \to \tau^+\tau^-$ are considered in the low Higgs mass searches. $H \to W^+W^-$ is the only decay channel considered by CDF in the high mass searches. The following sections will present brief descriptions of these searches and their latest results. Because no evidence for SM Higgs boson production has been observed, CDF has set 95% C.L. upper limits on the production cross section times branching ratio for various test Higgs masses. All limits take into account the statistical and systematic uncertainties.

Table 1. The production and decay channels in the search for the SM Higgs boson considered by CDF in Run II.

Mass	Production	Higgs Decay	Non-Higgs Decays	Signature
	$q\bar{q}' \to W^* \to WH$	$H \to b\bar{b}$	$W \to l\nu$	lepton + $\not\!\!E_T$ + 2b jets
	$q\bar{q} \to Z^* \to ZH$	$H \to b\bar{b}$	$Z \to l^+l^-$	l^+l^- + 2b jets
	$W/Z + H$	$H \to b\bar{b}$	$W \to l\nu$, $Z \to \nu\bar{\nu}$ (charged lepton not not identified)	$\not\!\!E_T$ + 2b jets
Low	$W/Z + H$	$H \to b\bar{b}$	$W \to q\bar{q}'$, $Z \to q\bar{q}$	2q jets + 2b jets
	$W/Z + H$	$H \to \tau^+\tau^-$	$W \to q\bar{q}'$, $Z \to q\bar{q}$	2q jets + 2τ
	$q\bar{q}H$ (vector boson fusion)	$H \to \tau^+\tau^-$		2q jets(forward) + 2τ
	$gg \to H$	$H \to \tau^+\tau^-$		2τ
	$gg \to H$	$H \to W^+W^- \to l^+\nu l^-\bar{\nu}$		$l^+l'^-$ + $\not\!\!E_T$ (leptons may not be of same flavor)
High	$W/Z + H$	$H \to W^+W^- \to l^+\nu l^-\bar{\nu}$	W,Z: all decay channels	$l^+l'^-$ + $\not\!\!E_T$ + lepton(s) or jets
	$q\bar{q}H$ (vector boson fusion)	$H \to W^+W^- \to l^+\nu l^-\bar{\nu}$		$l^+l'^-$ + $\not\!\!E_T$ + jets
	$q\bar{q}' \to W^* \to WH$	$H \to W^+W^- \to l^+\nu l^-\bar{\nu}$	$W \to l\nu$	like-sign leptons + $\not\!\!E_T$

5.1. *Low Mass Higgs Boson Searches*

5.1.1. *Searches for the Higgs Boson in the $WH \to l\nu b\bar{b}$ Channel*

CDF has searched for the SM Higgs boson in the channel where the Higgs boson is assumed to be produced in association with a W boson. The search is focused on the signal events in which the W boson decays leptonically ($W \to e\nu$ or $W \to \mu\nu$) and the Higgs boson decays into $b\bar{b}$. Thus the final state signature consists of a high-p_T lepton (e or μ), a pair of b jets and large $\not\!\!E_T$ from the escaping neutrino. The integrated luminosity of the data sample used for the search is 2.7 fb^{-1} [26,27]. In each candidate event there should be an isolated lepton, two or more jets with transverse energy $E_T > 20$ GeV, and $\not\!\!E_T$ in the event greater than 20 GeV. The isolated lepton candidate can be a central electron ($|\eta_e| < 1$) or forward electron ($1.2 < |\eta_e| < 2.8$) of $E_T > 20$ GeV, a central muon ($|\eta_\mu| < 1$) of $p_T > 20$ GeV/c, or an isolated track of $p_T > 20$ GeV/c that is not matched to an electromagnetic energy cluster in the calorimeter nor to a muon stub in the muon chamber. At least one of the jets in the selected events is required to be tagged as a b jet candidate. The geometrical coverage of identifying a muon candidate at CDF with the requirement of an isolated track matching to hits in the muon chambers, can only detect muons up to $\mid \eta \mid < 1$. However the inclusion of an isolated track to be considered as a lepton candidate has helped to extend the muon identification coverage to $\mid \eta \mid < 1.2$, and it also helps to fill the gaps in the central region that are not covered by the muon chambers. This has increased the muon acceptance by $\sim 25\%$. Fig. 9 shows the gain in the muon acceptance, in the ϕ vs η plane, when CDF includes isolated tracks as lepton candidates.

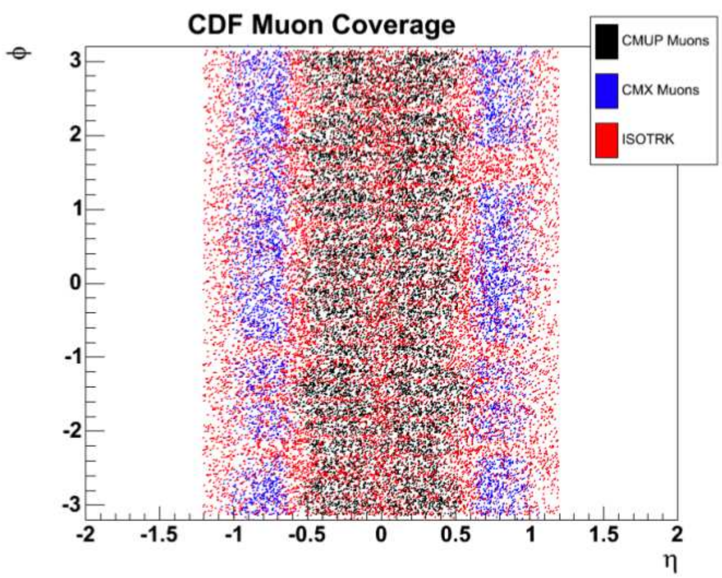

Fig. 9. The gain in the muon acceptance, in the ϕ vs η plane, when CDF includes isolated tracks as lepton candidates.

The main sources of background are from W boson production with heavy-flavor jets ($W + bb$, $W + cc$), Top quark pair production, electroweak production (single Top, di-boson), QCD multi-jet production that fakes a W production signature, and misidentification of non-b jets as b jets (mis-tag) in W boson production with light-flavor jets. The background due to misidentification of light-flavor jets as b jets is estimated by measuring the mis-tag rate in inclusive jets data samples. This mis-tag rate is applied to the data sample used for this Higgs boson search; i.e. the mis-tag rate is applied to each jet in events that have passed all selection cuts except the b jet tagging requirement. The contribution from QCD multi-jet production is estimated using the side-band data with low $\not\!\!E_T$, which is devoid of any signal, by extrapolating the background contribution into the signal region that is at higher $\not\!\!E_T$. The contributions from other background sources are estimated from simulations using theoretical next-to-leading-order (NLO) production cross sections for normalization.

The selected events are categorized into several exclusive groups based on the number of b jets identified by the SECVTX or the JET-PROBABILITY b jet tagging algorithm, and the type of identified charged lepton candidate. The selected events in each group are then sent through two trained multi-variate discriminant algorithms, an artificial neural network (NN) and a boosted decision tree (BDT), to discriminate between the possible signal events in the data from the background events. Separate trainings are performed for different Higgs boson test masses. For the neural network training, six kinematic variables per event are used to perform the signal and background separation. In the case of the boosted decision tree training, 21 event kinematic variables are used. These variables contain properties of the signal that can help to distinguish it from some of the backgrounds. For example among some of the common variables used in the NN and BDT trainings, the di-jet invariant mass distribution will be a resonance for the Higgs signal, whereas for most of the background it would be a continuous flatter distribution, except for the backgrounds with $Z \to q\bar{q}$. In the WH signal, both the W and H bosons are heavy particles. Therefore the total transverse energy ($H_t = \sum E_T(\text{jets}) + \not\!\!E_T + E_T/p_T(\text{lepton})$) of the signal events will generally be larger than background events from W+jets and QCD multi-jet. The $\not\!\!E_T$ in the WH signal is due to the neutrino from the $W \to l\nu$ decay. Thus the angular separation between the $\not\!\!E_T$ direction and the lepton direction in the signal will be different with respect to the non-W backgrounds.

The NN and BDT output distributions for one test Higgs mass is shown in Fig. 10. From the plots one can see that most of the background events are populated on the low end of the distributions, whereas the Higgs signal is predominantly populated on the high end of the distributions.

For each of the selected event groups, the observed NN and BDT output distributions from the data agree with the distributions from the predicted background contributions. Given no evidence for a Higgs signal we set limits on its production cross section times branching ratio. For the search using the NN discriminant technique, the observed upper limit at 95% C.L. on the WH production cross section times branching ratio ($\sigma(p\bar{p} \to WH) \times BR(H \to b\bar{b})$) varies between 3.6 and 62.9 times the SM predicted cross section for Higgs boson masses between 100 and 150 GeV/c^2. In the case of the search using the BDT discriminant algorithm, the observed limit varies between 3.5 and 108 times the SM prediction for Higgs boson masses between 100 and 150 GeV/c^2. The observed and expected limits on the WH production times branching ratio as a function of the Higgs boson mass is shown in Fig. 11 for the NN and BDT analyses.

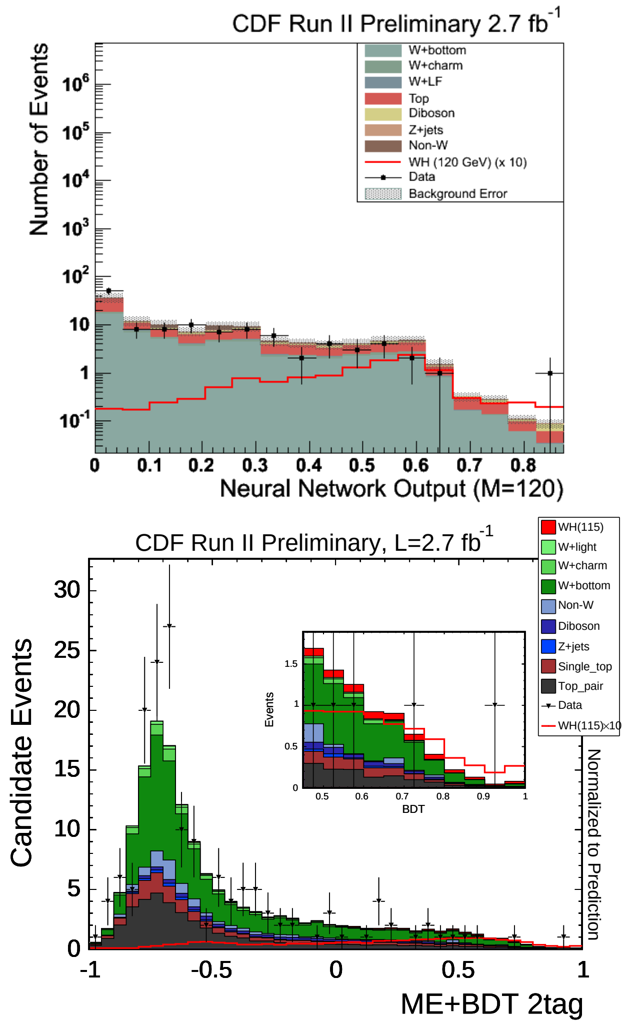

Fig. 10. (Top) Predicted and observed output for the neural network trained with a Higgs mass of 120 GeV/c^2 for events with a central lepton candidate and two b-tagged jets identified by SECVTX. (Bottom) Predicted and observed output for the boosted decision tree trained with a Higgs mass of 115 GeV/c^2 for events with two b-tagged jets identified by SECVTX. In both cases the signal distribution is multiplied by a factor of 10.

5.1.2. *Searches for the Higgs Boson in the $ZH \to l^+l^-b\bar{b}$ Channel*

At the Tevatron the Higgs boson can also be produced in association with a Z boson with a cross section roughly 1.6 times less than that of the WH production. CDF has searched for the Higgs boson in this production channel and in the decay modes of $Z \to l^+l^-$ $(l = e, \mu)$ and $H \to b\bar{b}$. The search is performed on a data sample of 2.4 fb^{-1} [28]. The events are first selected by requiring a pair of opposite charged

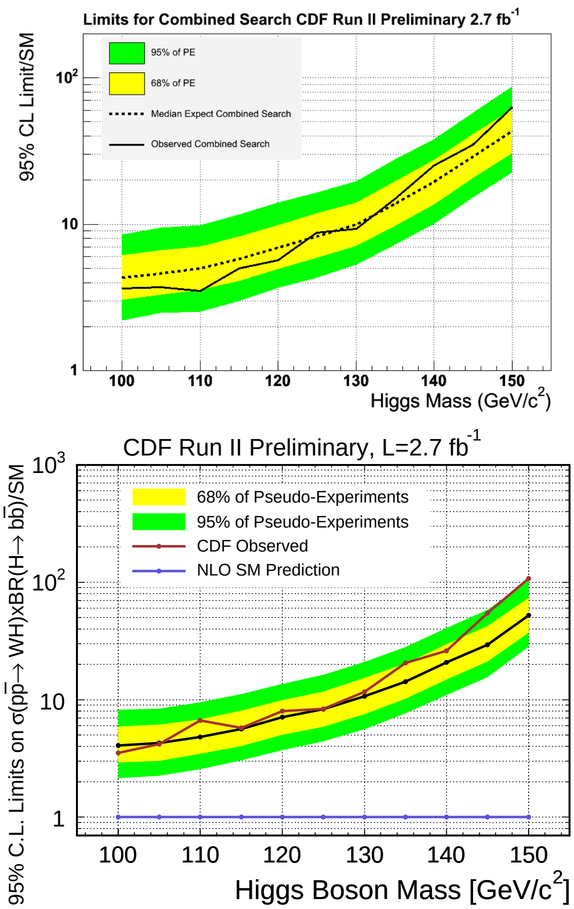

Fig. 11. Expected and observed limits on the Higgs production and decay for all lepton and b jet tag categories combined, as a function of the Higgs mass hypothesis for the search channel $WH \to l\nu b\bar{b}$. (Top) Results from the neural network analysis and (Bottom) results from the boosted decision tree analysis. Note that the limits are given as a ratio to the theoretical SM cross section.

electrons or muons. For the e^+e^- pair, one of the electrons must be detected in the central EM calorimeter and the other electron can be detected in the central or forward EM calorimeter. For the $\mu^+\mu^-$ pair, both muons are required to be identified within $|\eta| < 1$. The lepton pairs are selected using tight or loose identification cuts in order to achieve a balance between maximizing the lepton identification and having good purity. The reconstructed invariant mass $m_{l^+l^-}$ must be within the range $76 < m_{l^+l^-} < 106$ GeV/c^2 (the $m_{l^+l^-}$ resolution is approximately 3 GeV/c^2 for both the e^+e^- and $\mu^+\mu^-$ channels). The selected events are required to have at least two jets with $E_T > 15$ GeV and $|\eta| < 2$, and with at least one of the jets' transverse energy being greater than 25 GeV. The event must also have one tight

b-tagged jet or two loose b-tagged jets identified by the SECVTX algorithm.

One of the advantages in performing the search in this $ZH \to l^+l^-b\bar{b}$ channel is that all the physics objects in the final state can be detected if they fall within the instrumented region. Thus the missing energy in such an event is mainly caused by mis-measurement of jets' energies due to the detector's energy resolution, or by the escaping neutrinos from the semi-leptonic decays of the B hadrons in the b jets. CDF uses the direction and magnitude of the $\not{E}_T$ to correct the measured jet energies, and thus improve their energy resolution [29]. For example in the ZH simulation sample the di-jet invariant mass, $m_{b\bar{b}}$, resolution improves from 18% to 11% after applying the correction using the $\not{E}_T$ information. This improvement is illustrated in Fig. 12 [29].

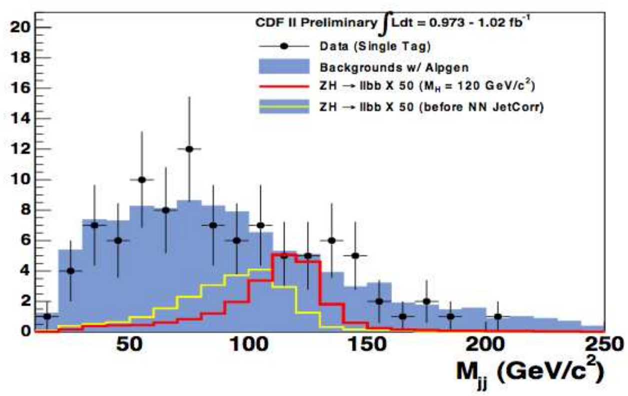

Fig. 12. The reconstructed di-jet invariant mass m_{jj} distribution from a CDF Higgs boson search in the $ZH \to l^+l^-b\bar{b}$ channel using a data sample with 1 fb^{-1}. The yellow histogram is the reconstructed $m_{b\bar{b}}$ invariant mass distribution of a ZH simulated sample, with $m_H = 120$ GeV/c^2, before applying the correction using the $\not{E}_T$ information. The red histogram is the reconstructed invariant mass after applying the correction.

The dominant sources of background to this search are the production of Z plus heavy-flavor jets (b or c jets), Z plus light-flavor jets with light-flavor jets mis-identified as b jets, $t\bar{t}$, ZZ, ZW, and events with fake leptons. The contributions from the Z plus heavy-flavor jets, $t\bar{t}$, ZZ and ZW are estimated with the ALPGEN [31] generator and using PYTHIA [32] to model the parton showers. The estimation of the background due to the mis-identification of light-flavor jets as b jets is done using the same technique as described in the $WH \to l\nu b\bar{b}$ search. The background from events with fake leptons is mainly coming from W+jets production where one of the leptons is a true lepton (from the W decay) and the other lepton is from a jet faking the lepton signature. The contribution from this background for the case of $Z \to \mu^+\mu^-$ is estimated from events with a like-sign di-muon pair. For the case of $Z \to e^+e^-$, CDF employs a data based fake rate method described in Ref. 30 to measure the fake background contribution.

The events that pass all the selected cuts are divided into four categories which are based on events with a single tight b-tagged jet, double loose b-tagged jets, lepton pairs passing tight identification cuts, or lepton pairs passing loose identification cuts. The JETNET [33] neural network algorithm is applied to the events in these four groups to discriminate possible signal events from the background events. Two neural networks are trained to separate between ZH signal and Z+jets background, and to separate between ZH signal and $t\bar{t}$ background. The purpose of having two separate neural network trainings is because Z+jets and $t\bar{t}$ are the two most dominant backgrounds, but are quite different from each other. Therefore, by having separate NN trainings one will be able to get the maximum discrimination between the Higgs signal and these two types of backgrounds.

The neural network output distributions from one of the four event categories are shown in Fig. 13. For each of the selection categories, the number of observed events in the data is consistent with the number of expected background events, and the observed neural network output distribution is also consistent with the expected neural network output distribution. Thus there is no evidence of a Higgs signal in the data. The observed (expected) upper limit at 95% C.L. on the ZH production cross section times branching ratio ($\sigma(p\bar{p} \to ZH) \times BR(H \to b\bar{b})$) varies between 8.8 (9.6) and 105 (105) times the SM prediction for Higgs boson masses between 100 and 150 GeV/c^2. These results are shown in Fig. 14.

5.1.3. *Searches for the Higgs Boson in the* $\not\!\!E_T + b\bar{b}$ *Channel*

CDF also considers a search for associated Higgs production using a final state of $\not\!\!E_T + b\bar{b}$, which is mostly sensitive to the signal of $ZH \to \nu\bar{\nu}b\bar{b}$. The search also has some sensitivity to $WH \to l\nu b\bar{b}$ where the charged lepton is not identified, or an electron that does not pass the electron identification selection is classified as a jet, or finally a tau lepton that decays hadronically can be reconstructed as a jet. For both production channels the Higgs decay considered is $H \to b\bar{b}$. The analysis is performed on a data sample of 2.1 fb^{-1} [34].

The main sources of background are from the production of W or Z bosons with jets, single Top quarks, $t\bar{t}$, and di-bosons. In these processes, the $\not\!\!E_T$ is mostly the result of neutrinos escaping detection. QCD multi-jet production is another source of background. In this case the $\not\!\!E_T$ is due to the mis-measurement of the energy of one or more jets, and the direction of the $\not\!\!E_T$ will tend to point in the direction of the mis-measured jet.

The pre-tag event selection cuts consist of requiring $\not\!\!E_T > 50$ GeV, two or three reconstructed jets with at least one jet located in the central calorimeter, and with the two leading jets spatially well separated ($\Delta R(jet_1, jet_2) > 1.0$). In addition there is a requirement of a minimal azimuthal distance between the $\not\!\!E_T$ and jets to suppress the QCD multi-jet background, and lastly it is required there be no reconstructed electron or muon candidate.

As with the other low mass Higgs searches, the signal contains a large fraction

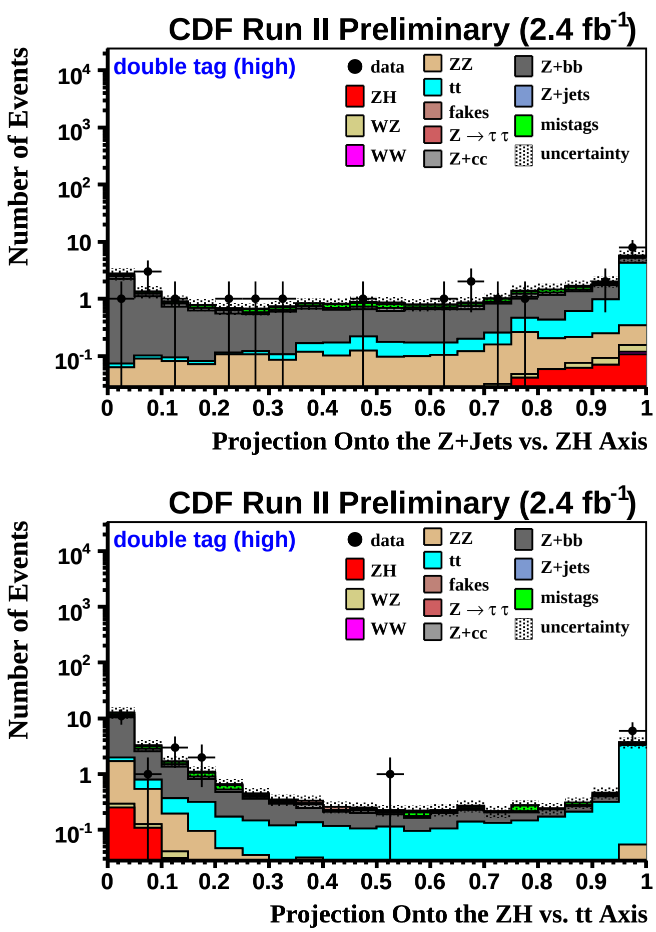

Fig. 13. Predicted and observed neural network output distributions for events with double loose b-tagged jets and lepton pairs passing tight identification cuts. (Top) Neural network trained to separate between Z+jets background and ZH signal, and (Bottom) Neural network trained to separate between $t\bar{t}$ background and ZH signal.

of b jets compared to the background, which is dominated by light-flavor jets. To enhance the signal over background, CDF identifies the b jets by employing both the SECVTX and JET-PROBABILITY b-tagging algorithms. The b-tagged samples are subdivided into three categories :

- two tight b-tagged jets identified by the SECVTX algorithm,
- one tight SECVTX tagged b jet and one loose JET-PROBABILITY tagged b jet,
- exactly one tight SECVTX tagged b jet.

To estimate the background contributions, the PYTHIA generator is used to model the production of W plus heavy-flavor jets, Z plus heavy-flavor jets, sin-

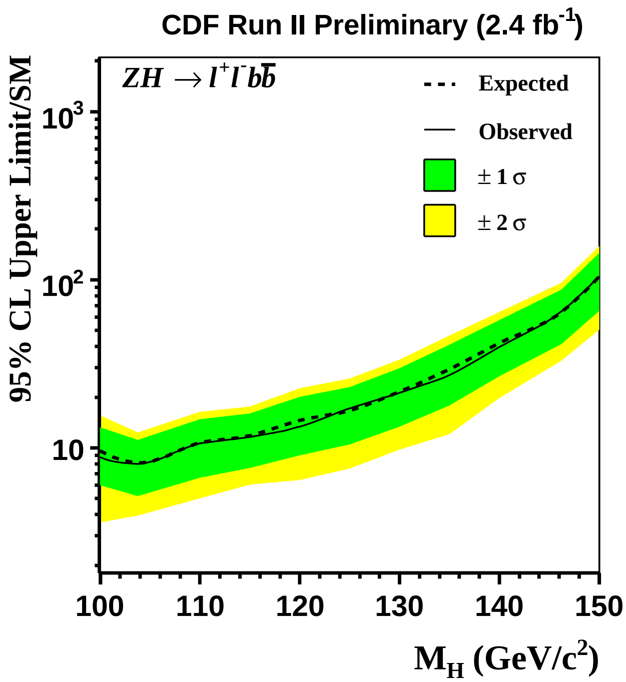

Fig. 14. Expected and observed cross section limits on Higgs production as a ratio of the theoretical SM value for all lepton and b jet tag categories combined, as a function of Higgs mass for the search channel $ZH \to l^+l^-b\bar{b}$.

gle top, $t\bar{t}$, and di-boson production. The contributions from the QCD multi-jet and the background from the misidentification of light-flavor jets as heavy-flavor, are determined by a data driven method, called the Tag Rate Matrix (TRM). In this section both types of background are together referred to as multi-jet background. To estimate the multi-jet background in the single-tagged sample, CDF measures the probability to tag one jet as a b jet from a pre-tag sample. Similarly, to estimate the multi-jet background in the double-tagged samples, CDF measures the probability to tag a jet as a b jet in a sample that already has one b-tagged jet. These probabilities are measured in sub-samples of the $\not\!\!E_T$+jets data set that are orthogonal to the signal sample. They are applied to the pre-tag signal data sample to predict the single-tagged multi-jet background, and applied to the signal data sample that already has one or more b-tagged jets to predict the double-tagged multi-jet background. A correction is applied to the predicted multi-jet background to remove the double counting of the non-multi-jet background. CDF then tested this method of predicting the total background in other kinematic control regions that are devoid of Higgs signal. The tests showed that the predicted background rates agree well with those observed in these non-signal regions, as shown in Fig. 15.

At this point in the analysis the most dominant background is QCD multi-jets.

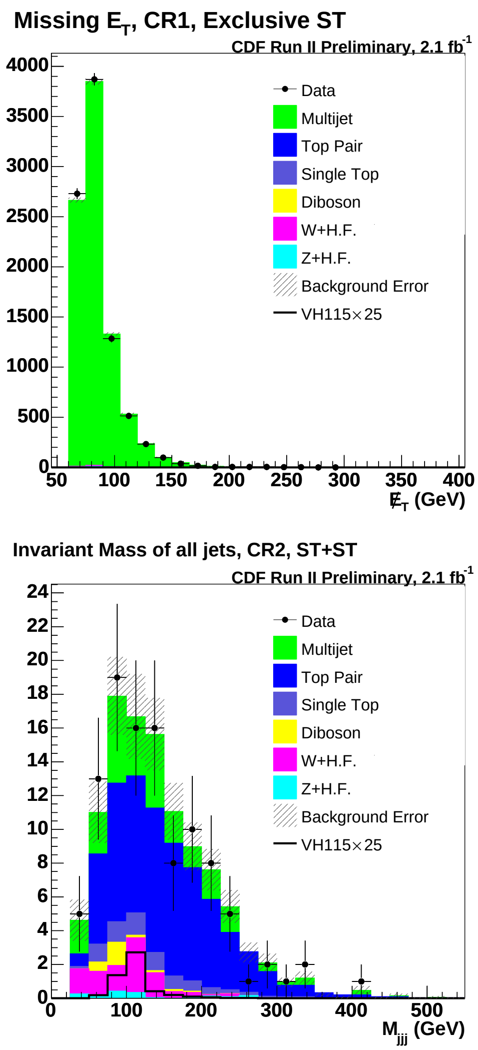

Fig. 15. Test of background predictions in the search of the SM Higgs boson in the $\not\!\!E_T + b\bar{b}$ channel. (Top) The $\not\!\!E_T$ distribution in a QCD multi-jet dominant region with one tight SECVTX tagged b jet. (Bottom) The invariant mass of the two-jet or three-jet system in a control region that has at least one identified charged lepton candidate and with two tight SECVTX tagged b jets. In both plots the solid black points are the observed data and the filled histograms are the predicted backgrounds.

To reduce this background CDF trained a NN (QCD_NN) on each of the three categories of b-tagged events, to distinguish QCD multi-jet events that have very different properties with respect to the signal and the other remaining backgrounds. The QCD_NN output distributions for the double-tagged events where one jet is tagged by the "tight" SECVTX algorithm and the other jet is tagged by the "loose"

JET-PROBABILITY algorithm, is shown in Fig. 16(Top). From the distribution one can see that the low QCD_NN region (QCD_NN < 0) is dominated by the QCD multi-jet background. Therefore, to further reduce the QCD multi-jet contribution CDF requires the events in the three categories of b-tagged events to have QCD_NN > 0. CDF then employs an addition NN algorithm to discriminate the surviving more signal-like background events against the Higgs signal. Seven kinematic variables are used in the training. Some of these kinematic variables include the maximum spacial separation (ΔR) between the two leading jets, the minimum azimuthal distance between the directions of the $\not\!\!E_T$ and the jets, the scalar sum of the transverse energy of the jets, and the invariant mass of the two-jet or three-jet system (m_{jj} or m_{jjj}). Fig. 16(Bottom) shows the NN output distribution of the double-tagged events where two jets are tagged by the "tight" SECVTX algorithm. In this plot the backgrounds are mostly populated at the low NN values, whereas the predicted Higgs signal is populated at the high NN values.

For each of the three b-tagged categories, the number of observed events in the data is consistent with the number of expected background events, and the observed NN output distributions are also consistent with the expected background NN output distribution. Again with there being no evidence of a signal, 95% C.L. limits are calculated for the signal production cross sections. The observed (expected) limit varies between 6.2 (5.2) and 63 (47) times the SM prediction for Higgs boson masses between 105 and 150 GeV/c^2, and are shown in Fig. 17.

5.1.4. *Searches for the Higgs Boson in the All-Hadronic Channel*

CDF has also performed a search for low mass Higgs bosons from WH/ZH production where both W or Z boson decays hadronically ($W \to qq'$, $Z \to q\bar{q}$) and the Higgs boson decays into a pair of b quarks [35]. The final state signature consists of four jets with at least two b jets. An advantage of this search channel compared to the searches described earlier is that the hadronic decay branching fractions of the W and Z bosons are larger than the leptonic decay branching fractions. However, a significant disadvantage is that it suffers from a large background contribution from QCD multi-jet production, making it an extremely challenging search channel.

The events are selected from a multi-jet triggered data sample with an integrated luminosity of 2 fb^{-1}. The selection cuts require the events to have at least four jets with two jets tagged as b jets by the tight SECVTX b jet tagging algorithm. The signal region is defined inside the mass ranges: $35 < m_{qq} < 120$ GeV/c^2 and $m_{bb} > 75$ GeV/c^2, where m_{qq} is the invariant mass of the two leading non-b tagged jets, and m_{bb} is the invariant mass of the two b tagged jets. The mass resolution of m_{qq} for $W \to qq'$ and $Z \to q\bar{q}$ are approximately $\sim 15\%$.

The dominant background is from QCD multi-jet production with heavy-flavor jets in the final state. Its contribution is estimated from a multi-jet data sample which has passed the same event selection cuts of the analysis except that only one jet is required to be tagged as a b jet in each event. These selected events are

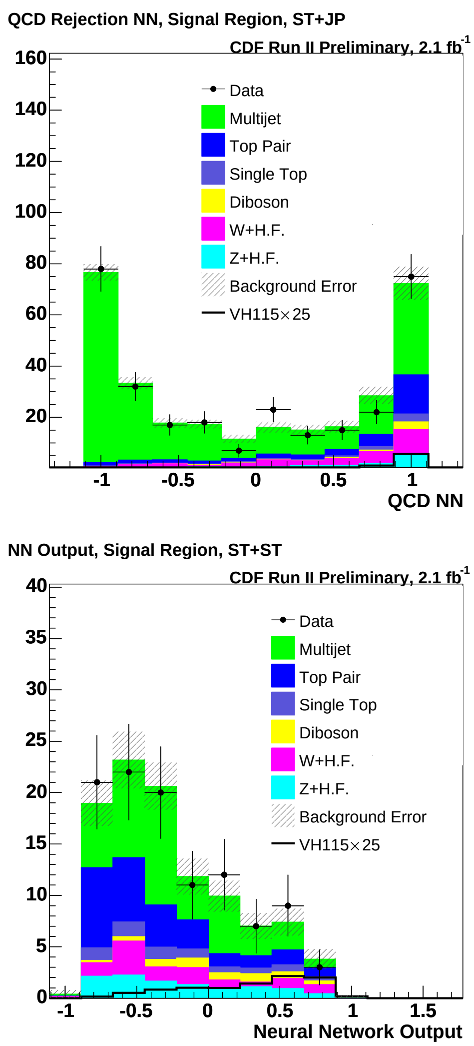

Fig. 16. (Top) Output from a neural network, which is trained to separate QCD multi-jet background from the non-QCD multi-jet backgrounds and Higgs signal, for events with one jet tagged by tight SECVTX algorithm and another jet tagged by loose JET-PROBABILITY algorithm. (Bottom) Output from a neural network, which is trained to separate the remaining QCD multi-jet and non-QCD multi-jet backgrounds from the Higgs signal, for events with two tight SECVTX b-tagged jets. The Higgs signal distributions are for a Higgs mass of 115 GeV/c^2.

then scaled by the probability that a second jet in the event would be tagged as a b jet, following the same TRM technique as in the SM Higgs boson search in the $\not\!\!E_T + b\bar{b}$ channel. The probability is measured in a control kinematic region outside the signal region.

In order to distinguish between signal and background events, CDF uses the log

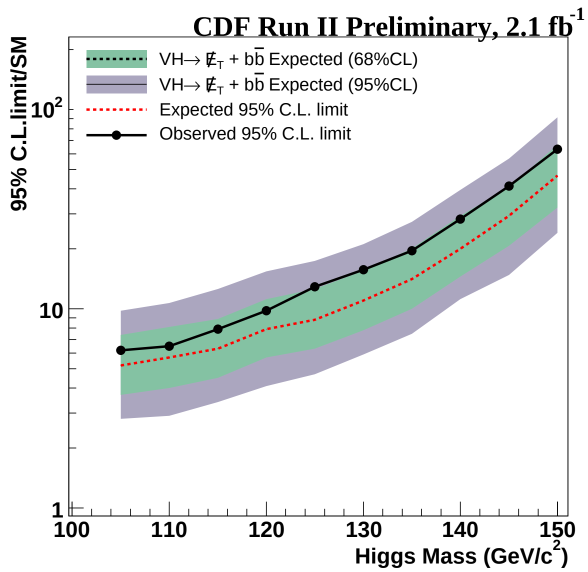

Fig. 17. Expected and observed limits on the Higgs production and decay as a function of the Higgs mass hypothesis for the search channel $\not{E}_T + b\bar{b}$.

likelihood ratio

$$Q = log\left(\frac{P(\mathbf{x} \mid \mathbf{WH}) + \mathbf{P}(\mathbf{x} \mid \mathbf{ZH})}{P(\mathbf{x} \mid \mathrm{QCD})}\right), \tag{2}$$

where $\mathbf{x}$ is the vector of measured jet momenta, and $P(\mathbf{x} \mid \mathbf{WH})$, $P(\mathbf{x} \mid \mathbf{ZH})$ and $P(\mathbf{x} \mid \mathbf{QCD})$ are the probabilities of observing the event with $\mathbf{x}$ for WH, ZH and QCD processes respectively. The probabilities are calculated using a Matrix Element technique which is described in more detail in Ref. 35.

The distributions of the discriminant Q for the expected background contributions and for the observed data are shown in Fig. 18. There is a good agreement over the full range and no evidence of a WH/ZH signal. The observed (expected) upper limit at 95% C.L. on the WH/ZH production cross section times branching ratio varies between 28 (29) and 105 (115) times the SM prediction for Higgs boson masses between 100 and 140 GeV/c^2.

5.1.5. *Searches for the Higgs Boson in the Di-Tau and Jets Channel*

At low Higgs mass the predicted $H \to \tau^+\tau^-$ branching ratio is about 10% (see Fig. 7). Although it is $\sim 8\times$ smaller than $BR(H \to b\bar{b})$, this decay mode provides another channel to search for the Higgs boson which is statistically independent from the search channels that are based on $H \to b\bar{b}$. CDF has performed a simultaneous search for the Higgs boson in various channels where the Higgs boson decays into

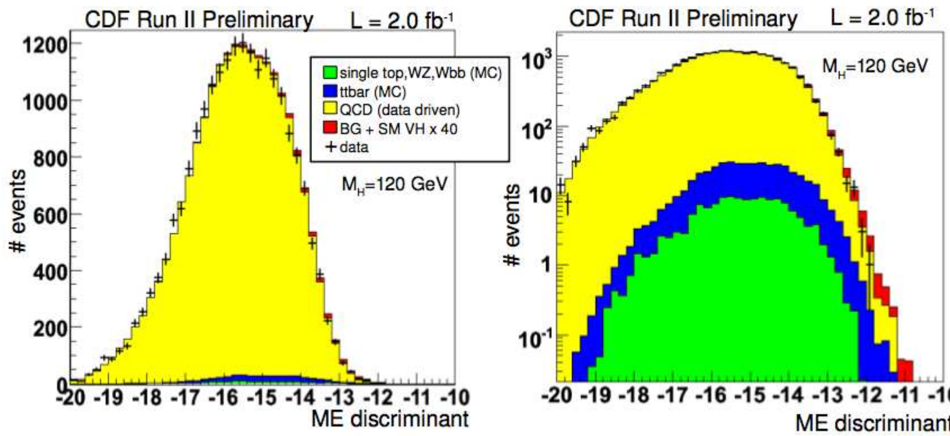

Fig. 18. Predicted and observed distributions of the matrix element discriminant in the signal region in 2.0 fb^{-1} data for the all-hadronic search channel.

a pair of tau leptons [36]. The final state signature that is focused on is $2\tau + 2$jets. The signal channels contributing to this final state are:

- $q\bar{q}' \rightarrow W(\rightarrow q\bar{q}')H(\rightarrow \tau^+\tau^-)$
- $q\bar{q} \rightarrow Z(\rightarrow q\bar{q})H(\rightarrow \tau^+\tau^-)$
- vector boson fusion: $qq \rightarrow qqH(\rightarrow \tau^+\tau^-)$
- gluon-gluon fusion: $gg \rightarrow H(\rightarrow \tau^+\tau^-)$, where the additional jets come from initial state QCD radiation.

The Feynman diagrams of these processes are shown in Fig. 19. CDF requires two or more jets in the final state of the gluon-gluon fusion production process because the signal's sensitivity over the background is worse for the cases where there are no jets or only one jet in the final state.

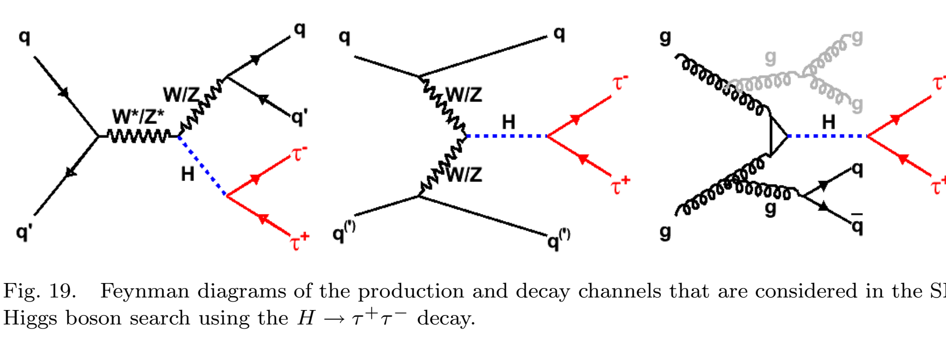

Fig. 19. Feynman diagrams of the production and decay channels that are considered in the SM Higgs boson search using the $H \rightarrow \tau^+\tau^-$ decay.

The search is performed on a data sample with an integrated luminosity of 2 fb^{-1}. The signal events are selected by requiring that there are two tau candidates and two jets with $E_T > 15$ GeV and $| \eta_{jet} |< 2.5$ in the final state. The tau lepton can decay leptonically (τ_{lep}) with branching ratio of $\sim 35\%$, or decay hadronically (τ_{had}) with branching ratio of $\sim 65\%$. For this analysis, CDF has chosen to search for the Higgs boson in the decay channel $\tau_{lep}\tau_{had}$ where one tau lepton decays leptonically and the other tau lepton decays hadronically. This is because this channel ($\tau_{lep}\tau_{had}$) has a relatively large decay branching ratio ($BR \sim 45\%$). The $\tau_{lep}\tau_{lep}$ decay channel has a small branching ratio of $\sim 12\%$, but a large background contribution from Drell-Yan production. The $\tau_{had}\tau_{had}$ decay channel has a relatively large decay branching ratio ($BR \sim 43\%$), however its final state signature will have a large background contribution from the QCD multi-jet production since a significant challenge in this analysis is to discriminate hadronically decaying taus from QCD jets. In this search, the leptonic tau candidate is either an isolated electron with $E_T > 10$ GeV, or an isolated muon with $p_T > 10$ GeV/c. The hadronic tau candidate is identified as a narrow isolated jet with low track multiplicity [37]. The τ_{lep} and τ_{had} candidate pair are also required to have opposite electric charge.

The main backgrounds are from the production of $W +$ jets, $Z +$ jets, $t\bar{t}$, dibosons ($WW/WZ/ZZ$) and QCD multi-jets. From $Z+$jets production, there is an irreducible background from $Z(\rightarrow \tau^+\tau^-)+$jets. For $W+$jets production, the lepton from the W boson decay can be identified as the τ_{lep} and one of the jets can fake the τ_{had} candidate. In QCD multi-jet production, one jet can be misidentified as an electron or muon, and another jet can fake a τ_{had} candidate. Most of the background contributions are estimated from simulations. The data events that contain a $\tau_{lep}\tau_{had}$ pair that have the same sign charge are used to model the contributions from the QCD multi-jet and a portion of the $W +$ jets contribution. The reason is that in QCD multi-jet production there is no charge correlation between the τ_{lep} and τ_{had} candidates. Therefore the contributions from opposite sign and same sign should be similar. For $W+$jets production, there is a charge correlation between the lepton from the W boson decay and the out-going quark. Thus, the contribution from opposite sign will be larger than from the same sign. To account for the contributions that are not in the same sign data events, CDF uses simulations to obtain the additional background contributions. After applying all the selection cuts, the observed number of events in the data is consistent with the predicted background events.

In order to improve the search sensitivity, a NN algorithm is used to discriminate the signal from the background. The signal consists of the four Higgs production processes mentioned earlier. Individual NN trainings are performed to discriminate the signal from three types of backgrounds :

- $Z(\rightarrow \tau^+\tau^-) +$ jets,
- $t\bar{t}$,
- QCD multi-jet.

Appropriate sets of kinematic variables are used for each type of training. The NN output distributions for the expected background, observed data, and the predicted

Higgs signal, of the three trained NNs are shown in Fig. 20. For each of the three NN trainings, the observed NN output distributions are consistent with the distributions from the expected background. For each event, a minimum NN score is picked from one of the three NN outputs to obtain the final NN discriminating distribution. The final NN distributions for the expected background, observed data, and the predicted Higgs signal are shown in Fig. 21. Again, the observed NN output distribution is consistent with the distribution from the expected background. There being no evidence of a Higgs signal, a one dimensional binned maximum likelihood fit is performed on the final NN output distributions to obtain 95% C.L. limits relative to the SM predictions. The observed (expected) limit on the SM Higgs boson production cross section times branching ratio ranges from 30 (24) to 159 (112) times the SM prediction for Higgs masses between 110 GeV/c^2 to 150 GeV/c^2. This is a new search at CDF and it is a novel analysis as it searches for the SM Higgs bosons in several production processes at the same time. The results from this search contributed about 10% to the total sensitivity of the combined CDF SM Higgs search (see section 5.3).

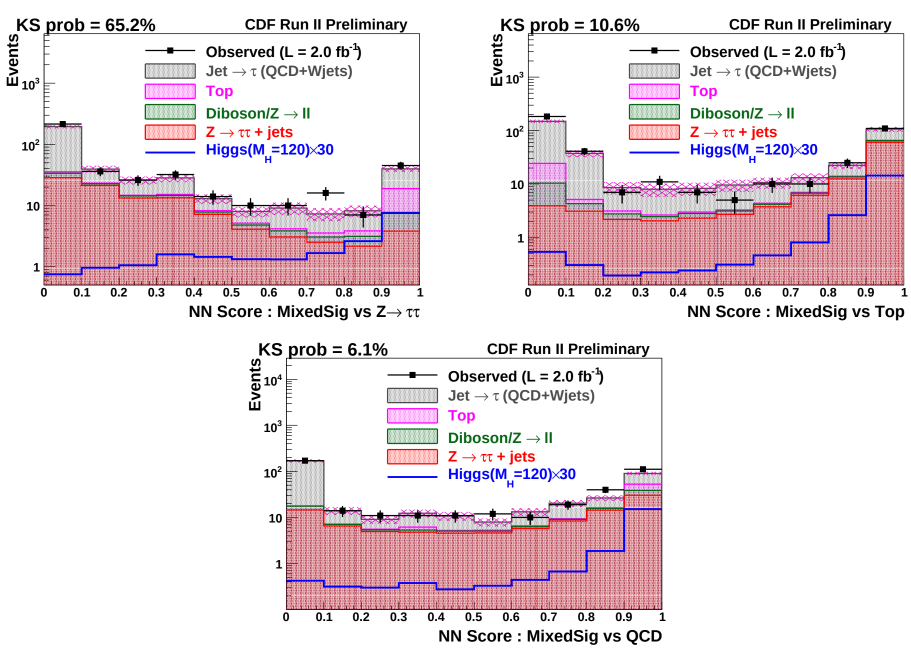

Fig. 20. Output distributions of the neural network which is trained to separate the Higgs signal from (Top-Left) $Z(\to \tau^+\tau^-)+$jets background, (Top-Right) $t\bar{t}$ background and (Bottom) QCD multi-jet background.

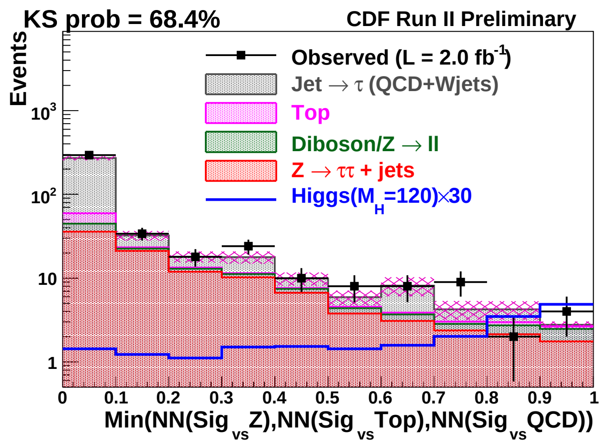

Fig. 21. Final neural network distribution after selecting the minimal score from one of the three neural network outputs.

5.2. *High Mass Higgs Boson Searches*

5.2.1. *Searches for the Higgs Boson in the $H \to W^+W^-$ Decay Channel*

The SM Higgs boson is predicted to decay predominantly into a pair of W bosons at high Higgs mass ($m_H \gtrsim 135$ GeV/c^2). This decay channel allows Higgs boson searches to take advantage of the $gg \to H$ production mechanism that has the largest predicted production cross section at the Tevatron compared to the other production processes, and does not suffer from the large QCD multi-jet background, which are faced in the low Higgs mass searches where the Higgs boson decays into a pair of b quarks. CDF has performed a search for the Higgs boson in this decay channel $H \to W^+W^- \to l^+\nu l^-\bar{\nu}$ using a data sample of 3 fb^{-1} [38]. The di-lepton pair combinations considered in this search are e^+e^-, $\mu^+\mu^-$ and $e^\pm\mu^\mp$. The final state of this decay mode provides a relatively clean channel for the Higgs search at the Tevatron as it has very small background contribution from the QCD multi-jet production. The Higgs production channels that CDF has considered in this search are gluon-gluon fusion ($gg \to H$), associated vector boson production (WH/ZH) and vector boson fusion ($qq \to qqH$).

The basic event selection consists of two isolated leptons of opposite charge. One of the leptons is required to have $E_T > 20$ GeV for an electron, or $p_T > 20$ GeV/c for a muon. The other lepton must have $E_T > 10$ GeV for an electron, or $p_T > 10$ GeV/c for a muon. The main sources of background are from $WW \to l^+\nu l^-\bar{\nu}$ production (the largest source of background and irreducible), $WZ \to l\nu ll$ production where one of the leptons is not identified, $ZZ \to l^+l^-\nu\bar{\nu}$ production, $t\bar{t} \to b\bar{b}l^+l^-\nu\bar{\nu}$ production, $W\gamma$ production where the photon is mis-identified as an electron, and $W+$jets production where one of the jets is mis-identified as a lepton. To suppress the Drell-Yan contribution, CDF requires $\not\!\!E_{T\,spec} > 25$ GeV where

$$\not\!\!E_{T\,spec} \equiv \begin{cases} \not\!\!E_T & \text{if } \Delta\phi(\not\!\!E_T, \text{nearest lepton or jet}) > \frac{\pi}{2} \\ \not\!\!E_T \sin\left(\Delta\phi(\not\!\!E_T, \text{lepton or jet})\right) & \text{if } \Delta\phi(\not\!\!E_T, \text{nearest lepton or jet}) < \frac{\pi}{2} \end{cases}$$

The cut on $\not\!\!E_{T\,spec}$ is a requirement that a significant amount of the missing transverse energy should not be due to the mis-measurement of the lepton or jet energies. If a lepton's energy or a jet's energy is mis-measured, the direction of the $\not\!\!E_T$ will tend to point in the direction close to the mis-measured lepton or jet. The di-lepton invariant mass is required to be $m_{l^+l^-} > 15$ GeV/c^2 to reduce the contribution from heavy-favor production. There is also a requirement of exactly two leptons to suppress the contribution from WZ production. The $t\bar{t}$ background is reduced by requiring that there is no b jet candidate tagged by the tight SECVTX algorithm.

The modeling of almost all the backgrounds are done with simulations. One exception is the $W+$jets background, it is estimated from a data sample in which each event has an identified lepton and at least one jet. The contribution of each event from this sample to the background of the Higgs search, is scaled by the probability that a jet is mis-identified as a lepton. The mis-identification probability is measured in a multi-jet data sample.

To improve the search sensitivity, a NN algorithm is used on the events that pass all the selection cuts to further separate the possible signal events from the background events. The NN training is performed separately for events with a final state that contains no reconstructed jet ("0jet"), one jet ("1jet"), or two or more jets ("$\geq$ 2jets"). This is done so that each NN can be optimally tuned to the different mixes of signal and background contributions in each jet multiplicity category. Some of the variables used in the NN trainings are the angular separation between the charged leptons ($\Delta R(l^+, l^-)$), the total event transverse energy ($H_t = \sum E_T(\text{jets}) + \not\!\!E_T + \sum E_T/p_T(l^+, l^-)$), the transverse energy of the leptons, and the angular separation between the $\not\!\!E_T$ direction and the direction of the l^+l^- system. The SM Higgs boson is a scalar particle, and when it is at rest and undergoes the decay $H \to WW^* \to l^+\nu l^-\bar{\nu}$, the two charged leptons tend to travel in the same direction to conserve helicity. At the Tevatron the produced Higgs boson will experience some boost which complicates the correlation of the leptons' directions. However the tendency for them to be closer together still remains. Conversely for the background, the angular separation between the charged leptons will be more uniformly distributed. Fig. 22 shows the distributions of $\Delta R(l^+, l^-)$ and H_t variables which are used in the NN trainings.

Once each NN has been trained, the NN output distribution templates are created for the signal, expected backgrounds and the observed data. The total number of observed events, the expected background and the predicted Higgs signal for a Higgs test mass of 160 GeV/c^2, are given in Table 2. The NN output distribution for the combined three jet categories is shown in Fig. 23. The number of events and the NN output distributions of the observed data are consistent with the expected background. To obtain Higgs production limits in this channel, CDF uses a binned

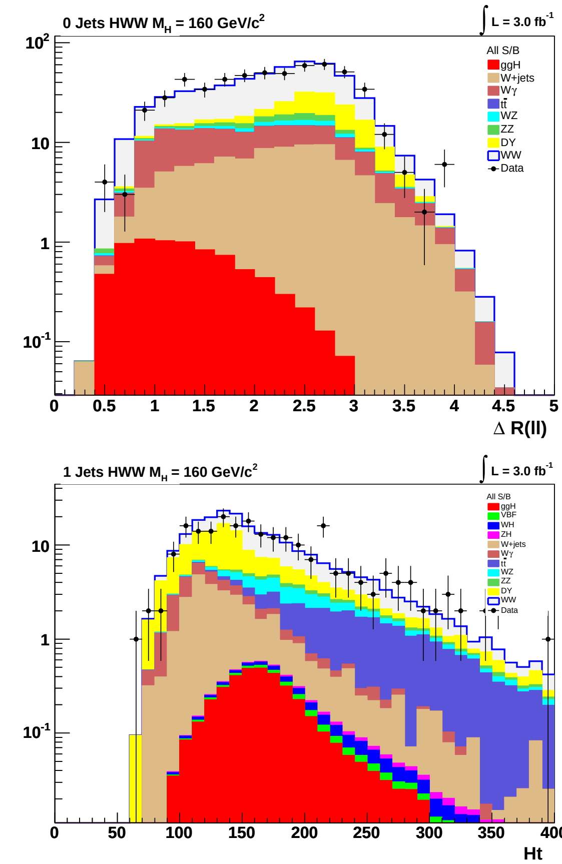

Fig. 22. Distributions of two of the seven variables used in the neural network trainings for the SM Higgs search in the $H \to WW^* \to l^+\nu l^-\bar{\nu}$ channel. (Top) Angular separation between the charged leptons in the "0jet" category. (Bottom) Total event transverse energy in the "1jet" category.

likelihood method to fit the NN output distributions from these three jet categories. In the fits, the expected background and the predicted signal are allowed to vary within a set of Gaussian constraints that are determined from the measured systematic uncertainties of the background and signal. The preliminary results of the ratio of the 95% C.L. production cross section limit to the SM prediction, as a function of the Higgs mass, is shown in Fig. 24. For a Higgs test mass of 160 GeV/c^2, the observed (expected) limit is 1.6 (1.7) times the SM prediction.

5.2.2. *Searches for the Higgs Boson in the Like-Sign Di-Lepton Channel*

At a hadron collider the expected contributions to a final state with like-sign high-p_T di-leptons ($l^\pm l^\pm$) is considerably smaller than for opposite sign di-leptons. One can expect relatively small background contributions when one performs searches

Table 2. The total number of observed events, the expected background and the predicted Higgs signal for Higgs mass of 160 GeV/c^2 in the search for the SM Higgs boson in the $H \to WW$ channel using a data sample of 3 fb^{-1}.

Events			
Number of jets	Expected Background	Observed	Predicted Higgs Signal ($m_H = 160$ GeV/c^2)
0	540 ± 65	552	8.4 ± 1.3
1	226 ± 28	227	5.2 ± 0.7
≥ 2	127 ± 20	139	3.9 ± 0.5

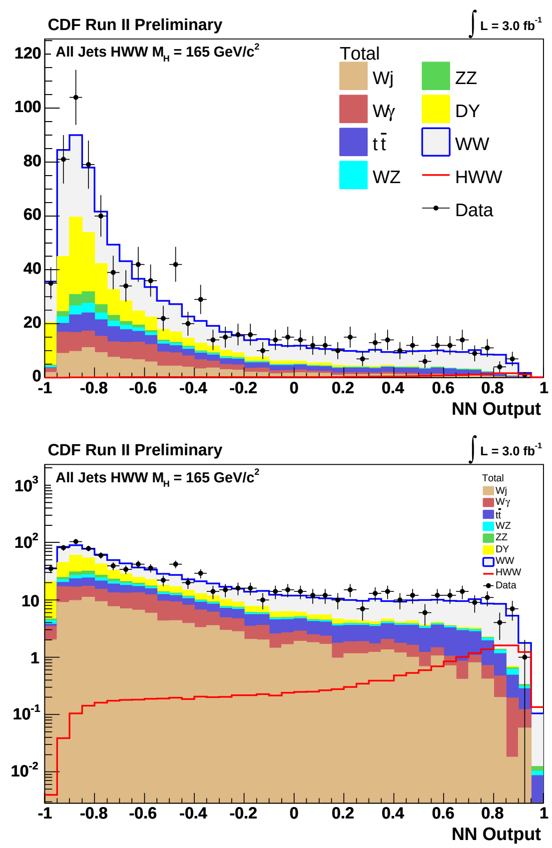

Fig. 23. Neural network distribution of the combined three jet categories in the search for the SM Higgs boson in the $H \to WW$ channel. The plot on the bottom is the same distribution using a logarithmic scale so that one can see the signal shape.

in a final state signature of like sign di-leptons. CDF has performed a search for the SM Higgs boson in this final state on a data sample of 1.9 fb^{-1} [39]. The production and decay channel considered for this search is $p\bar{p} \to WH \to WWW \to l^{\pm}l'^{\pm} + X$,

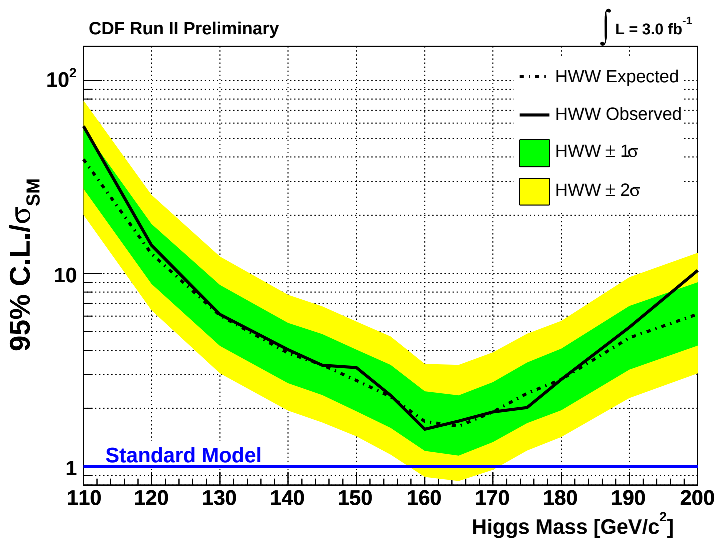

Fig. 24. The ratio of 95% C.L. production cross section limit to the SM prediction as a function of the Higgs boson mass.

and l is either an electron or muon. The events passing the baseline selection cuts should have at least one electron with $E_T > 20$ GeV or one muon with $p_T > 20$ GeV/c, and at least one electron with $E_T > 6$ GeV and $p_T > 6$ GeV/c or one muon with $p_T > 6$ GeV/c. The electron candidate should not be identified as one of the pair of electrons from a photon conversion. The two leptons must be located in the central region of the CDF detector ($| \eta |< 1$), originate from the same interaction vertex, and their invariant mass ,m_{ll}, should be larger than 12 GeV/c^2 but not consistent with the Z boson mass. Lastly, the charge of the two leptons must be of the same sign.

The dominant background sources are from events with one real lepton and the other identified lepton from either a jet faking the lepton or from photon conversion. The contribution from the fake lepton background is estimated by multiplying the number of lepton plus isolated track events observed in the data with fake lepton rates derived from inclusive jet data samples. The contribution from the photon conversion background is estimated by multiplying the number of observed data events with one lepton and an identified converted photon, with the residual photon conversion rate $R_{res} = \frac{1-\epsilon_{con}}{\epsilon_{con}}$, where ϵ_{con} is the efficiency to identify a converted photon. The remaining small background contributions from productions of Drell-Yan, di-bosons, $t\bar{t}$, and W bosons with heavy-flavor jets, are estimated with simulation. The total number of observed data events and expected background contributions after the baseline selection cuts are 134 and 142 ± 9, respectively. The final signal candidate events are selected by requiring the momentum of the second leading lepton to be $p_T > 20$ GeV/c and the momentum of the lepton pair to be

$p_T > 15$ GeV$/c$. After applying the final selection cuts, CDF observed 3 events and expected 3.3 ± 0.7 background events. The predicted number of SM Higgs signal events is 0.18 for a mass of 160 GeV$/c^2$.

With no evidence of Higgs signal, CDF determines the 95% C.L. upper limit on the cross section times branching ratio ($\sigma(p\bar{p} \to WH) \times BR(H \to WW)$) of SM Higgs boson production. The preliminary limit is shown in Fig. 25. For a Higgs mass of 160 GeV$/c^2$, the observed (expected) limit is 1.5 pb (1.6 pb), which is 33 (36) times the SM prediction. The plot in Fig. 25 also shows the predicted $\sigma(p\bar{p} \to WH) \times BR(H \to WW)$ for the production of the SM Higgs boson and the fermiophobic Higgs boson. Unlike the SM Higgs boson, the fermiophobic Higgs boson does not couple to fermions. Thus, at low Higgs mass, the fermiophobic Higgs boson decays pre-dominantly in the channel $H \to WW$. If a fermiophobic Higgs boson exists, it could indicate that the origin of particle masses would be different for bosons and fermions.

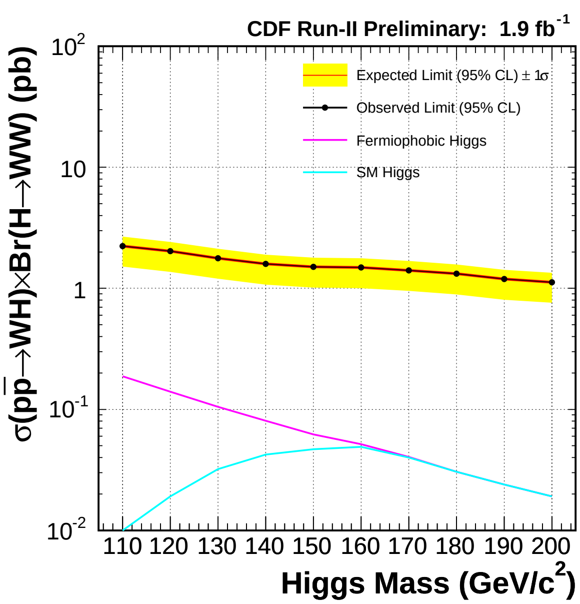

Fig. 25. The 95% C.L. upper limit on the production cross section times branching fraction as a function of the SM Higgs boson mass in the search of the SM Higgs boson using the like-sign di-lepton final state.

5.3. *Combined Results from all Searches*

In the earlier sections we presented the results on various searches for the SM Higgs boson by the CDF experiment. The search sensitivity varies among the channels.

Some have better sensitivity at low Higgs mass, whereas other channels have better sensitivity at high Higgs mass. As each search analysis explores different production and decay channels of the Higgs boson, one can greatly improve the search sensitivity by combining the results from all analyses. CDF has recently performed a combination [40] using the latest results from five analyses:

- $WH \to l\nu b\bar{b}$ ($\int Ldt = 2.7$ fb^{-1}) ,
- $ZH \to l^+l^-b\bar{b}$ ($\int Ldt = 2.4$ fb^{-1}) ,
- $WH/ZH \to \not\!\!E_T b\bar{b}$ ($\int Ldt = 2.1$ fb^{-1}) ,
- $H \to \tau^+\tau^-$ ($\int Ldt = 2.0$ fb^{-1}) ,
- $H \to WW$ ($\int Ldt = 3.0$ fb^{-1}) .

A Bayesian technique [41] is used to calculate the observed and expected limits of the combined results, assuming a flat prior for the total selected Higgs boson cross section. The results of the combination are given in Table 3 and in Fig. 26. For a Higgs mass of 115 GeV/c^2, the observed (expected) limit is 4.2 (3.6) times the SM prediction. Whereas for a Higgs mass of 160 GeV/c^2, the observed (expected) limit is 1.5 (1.7) times the SM prediction.

Table 3. Observed and expected limits for all CDF SM Higgs search channels combined using the Bayesian method.

m_H (GeV/c^2)	Observed limit/SM	-2σ expected	-1σ expected	median expected	$+1\sigma$ expected	$+2\sigma$ expected
100	3.01	1.43	2.07	3.13	4.78	7.10
105	2.87	1.30	1.91	2.98	4.62	6.95
110	3.34	1.47	2.15	3.29	5.00	7.35
115	4.19	1.58	2.32	3.56	5.43	8.05
120	4.53	1.93	2.75	4.15	6.29	9.31
125	6.04	1.87	2.77	4.29	6.55	9.72
130	5.62	1.99	2.80	4.21	6.38	9.46
135	5.40	1.58	2.29	3.52	5.42	8.12
140	5.45	1.48	2.20	3.41	5.23	7.79
145	3.92	1.33	2.02	3.11	4.71	6.90
150	4.13	1.12	1.65	2.60	4.08	6.20
155	2.27	1.19	1.63	2.30	3.24	4.52
160	1.52	0.86	1.17	1.68	2.43	3.50
165	1.64	0.80	1.12	1.60	2.26	3.13
170	1.80	0.98	1.33	1.90	2.73	3.88
175	1.97	1.22	1.63	2.35	3.45	5.03
180	2.52	1.35	1.89	2.74	3.95	5.60
185	4.47	1.90	2.64	3.81	5.48	7.76
190	5.47	2.15	3.11	4.54	6.50	9.09
195	9.05	2.64	3.62	5.33	7.94	11.63
200	10.18	2.92	4.15	6.19	9.22	13.44

The results of the SM Higgs boson searches from both the CDF and DØ experiments have also been combined. The combination performed in the winter of

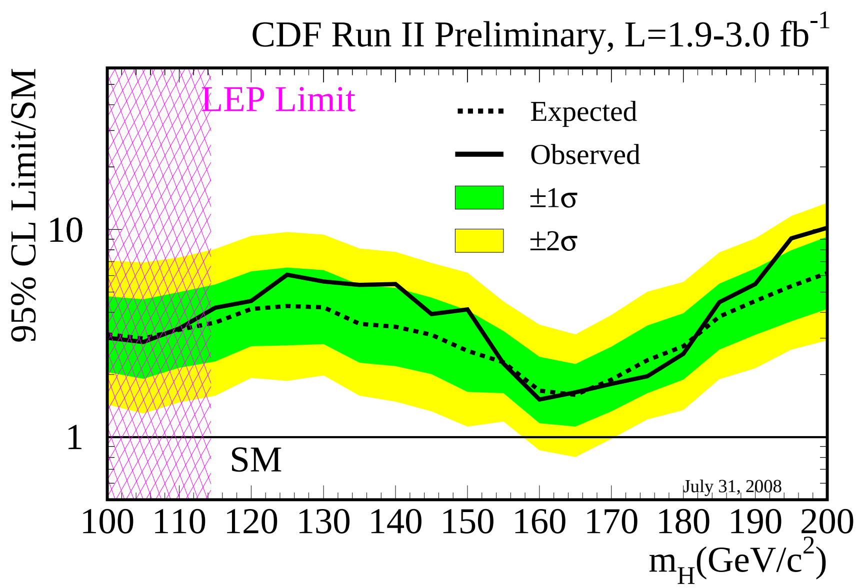

Fig. 26. The ratio of 95% C.L. production cross section limit to the SM prediction as a function of the Higgs mass, for the combination of all of CDF's SM Higgs search channels.

2008 [42] included results from both the low and high Higgs mass searches that were performed on data samples with integrated luminosities of 1 to 2.4 fb^{-1} from CDF and DØ. The combined observed (expected) limit for Higgs mass of 115 GeV/c^2 is 3.7 (3.3) times the SM prediction. For the Higgs mass of 160 GeV/c^2, the combined observed (expected) limit is 1.1 (1.6) times the SM prediction.

The most recent combination of the CDF and DØ SM Higgs search results was done in the summer of 2008 [43]. In this combination only the results from the high mass ($m_H > 155$ GeV/c^2) searches were used. The integrated luminosities of the corresponding data samples used in the searches range from 1.9 fb^{-1} to 3.0 fb^{-1}. The observed and expected limits are calculated using a Bayesian approach and assuming a flat prior for the Higgs boson cross section. The ratios of the 95% C.L. observed and expected limit to the SM cross section for various Higgs boson masses are given in Table 4 and in Fig. 27. The combined search results from CDF and DØ have excluded the production of a SM Higgs boson with mass of 170 GeV/c^2 at 95% C.L. . When using the CL_S method [43] for the limits calculation, the Higgs mass of 170 GeV/c^2 is also excluded at the 95% C.L., and the mass range of $\sim 163 - 177$ GeV/c^2 is excluded at the 90% C.L. . These are the first exclusions of the Higgs mass at a hadron collider.

Table 4. The ratios of the 95% C.L. observed and expected limit to the SM cross section for the combined CDF and DØ analyses as a function of the Higgs mass in GeV/c^2, obtained with the Bayesian method.

	155	160	165	170	175	180	185	190	195	200
Expected	1.7	1.3	1.2	1.4	1.7	2.0	2.8	3.3	4.2	4.6
Observed	1.7	1.4	1.2	1.0	1.3	1.6	2.5	3.3	4.8	5.1

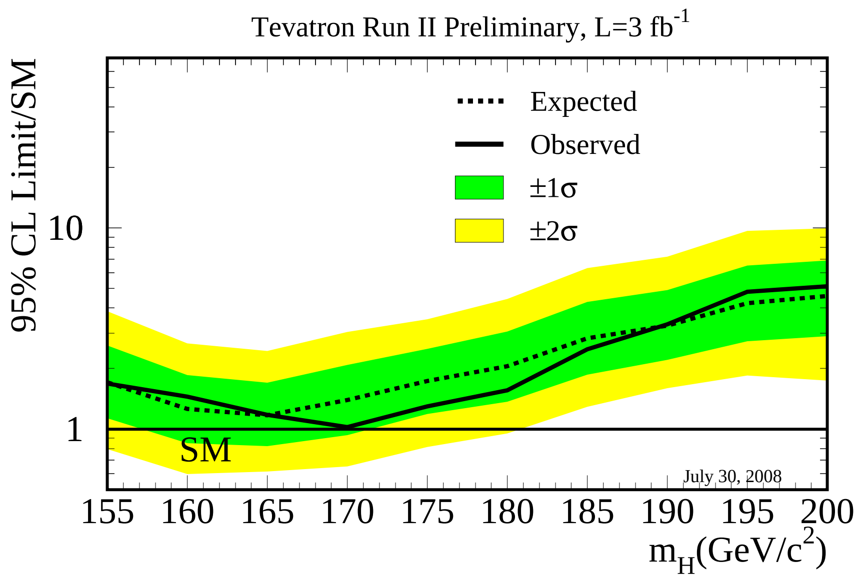

Fig. 27. The ratio of 95% C.L. production cross section limit to the SM prediction as a function of the Higgs mass, for the combined CDF and DØ analyses.

6. Searches for Non-Standard Model Higgs Boson at CDF

Earlier in the introduction we mentioned that a theory beyond the SM is needed to provide a fundamental explanation to the mechanism behind the electroweak symmetry breaking and to solve the naturalness problem. Several extensions to the SM have been developed to address these issues as well as other issues of the SM. Some of these extension models expand the Higgs sector and predict more than one kind of Higgs boson particle.

In the minimal supersymmetric extension of the SM (MSSM) two Higgs doublets are required, resulting in a Higgs sector with three neutral Higgs bosons ($\phi = h, H, A$) and two charged Higgs bosons (H^+,H^-). CDF has searched for the neutral

Higgs bosons in the decay modes $\phi \to b\bar{b}$ [44] and $\phi \to \tau^+\tau^-$ [45]. The charged Higgs are searched for in the case when CDF considers the possibility of the $t \to H^\pm b$ decay mode in addition to $t \to Wb$ for the measurement of the $t\bar{t}$ production cross section at the Tevatron [46]. So far CDF has not observed any evidence of the neutral and charged Higgs bosons predicted by the MSSM and has set limits on m_ϕ as function of $\tan\beta$ for the neutral Higgs searches, and on $m_{H^\pm}$ vs $\tan\beta$ and $BR(t \to H^\pm b)$ vs $m_{H^\pm}$ for the charged Higgs bosons search ($\tan\beta$ is the ratio of the vacuum expectation values of the two Higgs fields).

There are other models [47,48,49] that predict new Higgs doublets and triplets containing doubly-charged Higgs bosons ($H^{\pm\pm}$). At the Tevatron the doubly-charged Higgs boson is predicted to be produced mostly through the channel $p\bar{p} \to H^{++}H^{--}$. The $H^{\pm\pm}$ decays predominantly to charged leptons if $m_{H^{\pm\pm}} < 2m_{H^\pm}$ and $m_{H^{\pm\pm}} - m_{H^\pm} < m_W$. CDF has searched for the production of $H^{\pm\pm}$ in the same-sign ee, $e\mu$ and $\mu\mu$ [50] final states, and in the same-sign $e\tau$ and $\mu\tau$ [51] final states. Unfortunately no evidence of the doubly-charged Higgs boson signal was found. CDF has also searched for long-lived $H^{\pm\pm}$ boson, which would decay outside the detector. The results of the search is described in Ref. 52.

7. Projection and Prospects

Over the past few years CDF has improved its sensitivity on the search for the SM Higgs boson by increasing the data size used in the searches and by improving the analysis techniques. The improvement in the expected limits of the combined search for a Higgs boson with masses of 115 GeV/c^2 and 160 GeV/c^2 are shown in Fig. 28, where the x-axis of the plots are the total integrated luminosity of the data sample used in the search [40]. The curves in the figure are simple extrapolations of the expected limits by the function $1/\sqrt{\int Ldt}$ to approximate the improvement of the search sensitivity that may be achieved with only increasing the size of the search data sample. The improvement in the expected limit obtained by CDF surpasses what is expected from the $1/\sqrt{\int Ldt}$ dependence alone. This is due to the additional improvement in the analysis techniques used in the searches. These analysis improvements include increasing the signal acceptance by exploiting previously unused trigger paths and event topologies, as well as better discrimination of the signal and background through the use of advanced multi-variate algorithms. The yellow band in the plots are the projected sensitivity in the search performance relative to the summer 2007 sensitivity. The upper curve of the yellow band is the predicted improve sensitivity if one includes into the search analysis the improvement techniques that exist but are not yet used in the analyses. This gives a factor of 1.5 improvement in the sensitivity over the summer 2007. This factor of improvement has been achieved in the high Higgs mass search in summer 2008, and the low Higgs mass search is not far behind. The lower curve is the predicted further improvement of the sensitivity that may be achieved by including ideas that have not yet been tried, which is another factor of 1.5 improvement in the sensitivity.

Overall CDF could gain a total improvement factor of 2.25 over its summer 2007 sensitivity. In Fig. 28 one can see that by employing all the existing and potential improvement techniques, CDF may achieve the sensitivity of excluding a Higgs mass of 115 GeV/c^2 with a data sample of ~ 7 fb^{-1}.

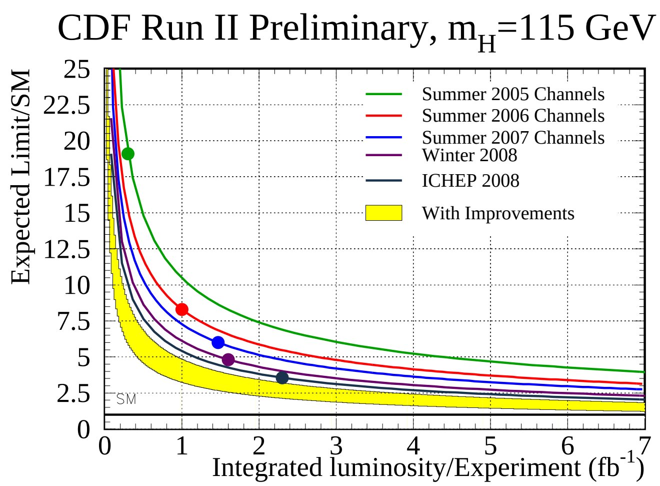

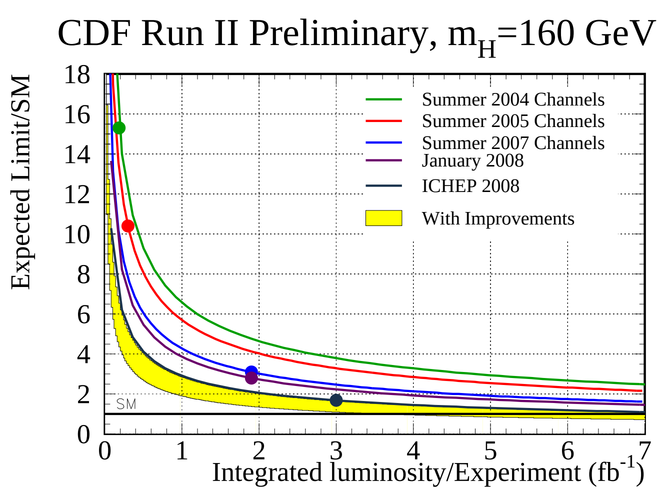

Fig. 28. The achieved and projected sensitivity for the combined CDF Higgs searches at (Top) $m_H = 115$ GeV/c^2 and (Bottom) $m_H = 160$ GeV/c^2. The solid circles are the achieved sensitivity, and the $1/\sqrt{\int L dt}$ curves are the projected improvement in the sensitivity with only increasing the size of the search data sample. The yellow bands indicate the projected sensitivity in performance, relative to the Summer 2007 sensitivity.

The plots in Fig. 29 show the probabilities for the Tevatron experiments to observe a two sigma exclusion, three sigma evidence and five sigma discovery of a Higgs boson of mass 115 GeV/c^2 and 160 GeV/c^2, as a function of the integrated luminosity per experiment [53]. The solid (dash) lines show the Higgs search sensitivities with a factor of 2.25 (1.5) improvement over the Tevatron's summer 2007 sensitivities. With an integrated luminosity of 7 fb^{-1} for each CDF and DØ experiment, and a factor of 2.25 improvement in the search sensitivities, Tevatron may have a 70% (95%) chance of excluding a Higgs mass of 115 (160) GeV/c^2 at the 95% C.L. , or 30% (75%) chance of observing a Higgs boson with mass 115 (160) GeV/c^2 at the three sigma level.

The projected Tevatron's sensitivity reach of the SM Higgs search as a function of the Higgs mass, is shown in Fig. 30 [54]. With an integrated luminosity of ~ 7 fb^{-1} per experiment, the Tevatron should be able to exclude most of the SM Higgs mass range up to 185 GeV/c^2 at 95% C.L. , if there is no SM Higgs boson in this range. If the mass of the SM Higgs boson is in this mass range, then the Tevatron may have a chance of observing a three sigma evidence of the Higgs boson within the mass range of $\sim 155 - 170$ GeV/c^2.

The LHC is expected to begin colliding proton on proton in 2009. The machine's designed center-of-mass energy is $\sqrt{s} = 14$ TeV. The ATLAS and CMS detectors have been optimized for the Higgs boson search. Both experiments are expected to be able to discover a SM Higgs boson with a mass range between 100 GeV/c^2 to 1 TeV/c^2 by performing the searches in various production and decay channels and with sufficient integrated luminosity. The predicted sensitivity of the SM Higgs search of the CMS experiment is shown in Fig. 31 [55].

8. Summary

The CDF collaboration has searched for the SM Higgs boson in various production and decay channels with data samples up to 3 fb^{-1}. No Higgs signal has been observed so far. By combining the results from all search channels, the observed 95% C.L. upper limit on the production cross section times branching fraction for a Higgs mass of 115 GeV/c^2 (160 GeV/c^2) is 4.2 (1.5) times the SM prediction. When the search results from CDF and DØ are combined, a Higgs mass of 170 GeV/c^2 is excluded at 95% C.L. , with the expectation that a window of excluded masees around 170 GeV/c^2 will grow in the coming months as further improvement are implemented. Both CDF and DØ are working on further improving search techniques. With an integrated luminosity of ~ 7 fb^{-1} from each experiment, it is possible that the combined result from CDF and DØ will exclude most of the SM Higgs mass range up to 185 GeV/c^2 at 95% C.L. .

Acknowledgments

I would like to thank our colleagues in the CDF and DØ collaborations for their outstanding work, and the Fermilab accelerator division for providing excellent colliding

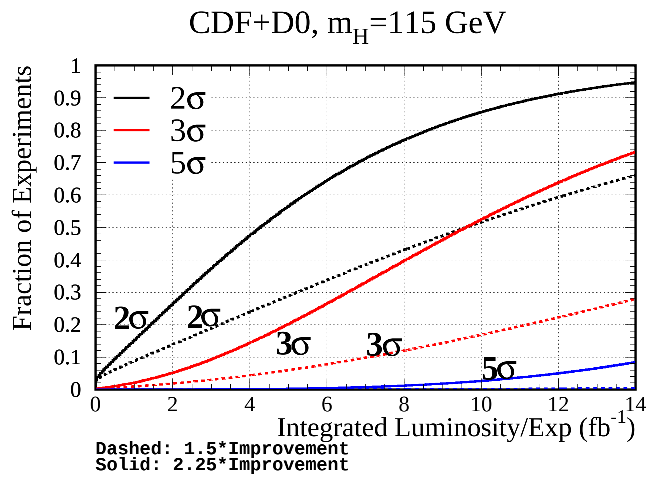

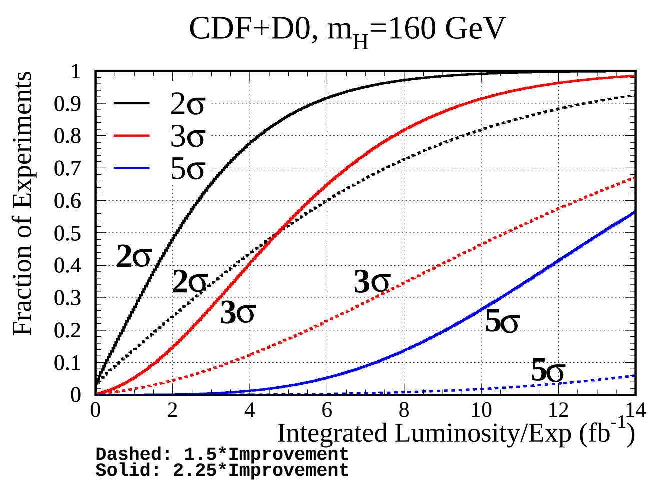

Fig. 29. Probabilities for the Tevatron experiments to observe a two sigma exclusion, three sigma evidence and five sigma discovery of a Higgs boson of mass (Top) 115 GeV/c^2 and (Bottom) 160 GeV/c^2, as a function of the integrated luminosity per experiment.

beams to each CDF and DØ experiment. I would also like to thank D. Glenzinski, M. Kruse, S. Lammel and A. Mitra for their careful reading of the manuscript. This work was supported by the National Science Council of the Republic of China.

References

1. CDF Collab. (F. Abe *et al.*), *Phys. Rev. Lett.* **74**, 2626 (1995); DØ Collab. (S. Abachi *et al.*), *Phys. Rev. Lett.* **74**, 2632 (1995).

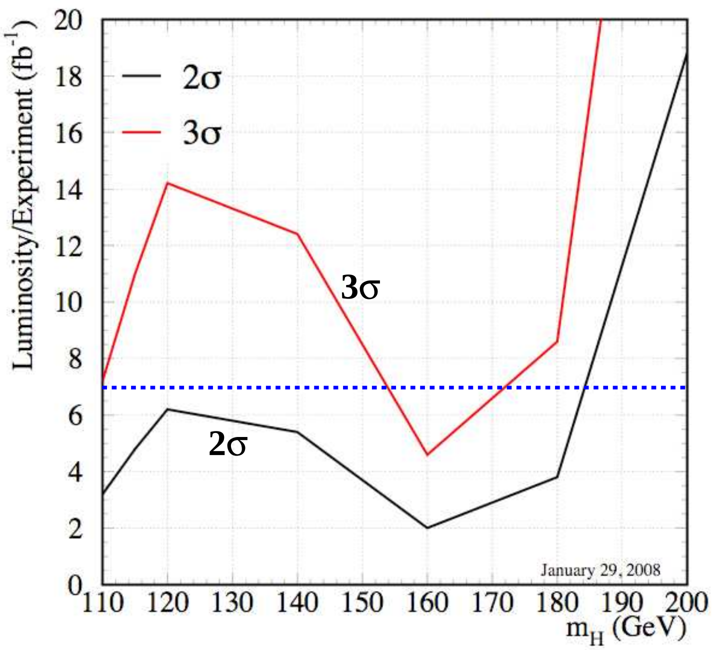

Fig. 30. The projected Tevatron's sensitivity reach of the SM Higgs search.

2. K. Kodama *et.al.*, (DONUT Collaboration), Phys. Lett. B **504**, 218 (2001).
3. K. Riesselmann, DESY-97-222 (1997) and in *arXiv:hep-ph/9711456*.
4. SINDRUM Collab. (S. Egli *et al.*), *Phys. Lett. B* **222**, 533 (1989); G.D. Barr *et al.*, *Phys. Lett. B* **235**, 356 (1990); CUSB Collab. (M. Sievertz *et al.*), *Phys. Rev. Lett.* **26**, 717 (1989); CLEO Collab. (M.S. Adam *et al.*), *Phys. Rev. Lett.* **40** 712 (1989); CUSB Collab. (J. Lee-Franzini *et al.*), *Proc. Int. Conf. High Energy Phys. XXIVth, Munich, Aug. 4-10, 1988*, p. 891 (1989).
5. ALEPH Collab. (R. Barate *et al.*), *Phys. Lett. B* **526**, 191 (2002).
6. DELPHI Collab. (J. Abdallah *et al.*), *Eur. Phys. J.* **C32**, 145 (2004).
7. L3 Collab. (M. Acciarri *et al.*), *Phys. Lett. B* **517**, 319 (2001).
8. OPAL Collab. (G. Abbiendi *et al.*), *Eur. Phys. J.* **C26**, 479 (2003).
9. the ALEPH Collaboration, the DELPHI Collaboration, the L3 Collaboration and the OPAL Collaboration, The LEP Working Group for Higgs Boson Searches, (G. Abbiendi *et al.*), *Phys. Lett. B* **565**, 61 (2003).
10. LEP Electroweak Working Group, status of July 2008, http://lepewwg.web.cern.ch/LEPEWWG/
11. M. Carena *et al.*, Report of the Tevatron Higgs Working Group, in *arXiv:hep-ph/0010338*.
12. M. Spira, Higgs Boson Production and Decay at the Tevatron, in *arXiv:hep-ph/9810289*.
13. A. Djouadi, J. Kalinowski and M. Spira, *Comput. Phys. Commun.* **108**, 56 (1998).
14. Fermilab Beams Division Collaboration, Run II Handbook, in *http://www-bd.fnal.gov/lug/runII_handbook/RunII_index.html*.
15. CDF Collab. (D. Acosta *et. al.*), *Phys. Rev. D* **71**, 032001 (2005).

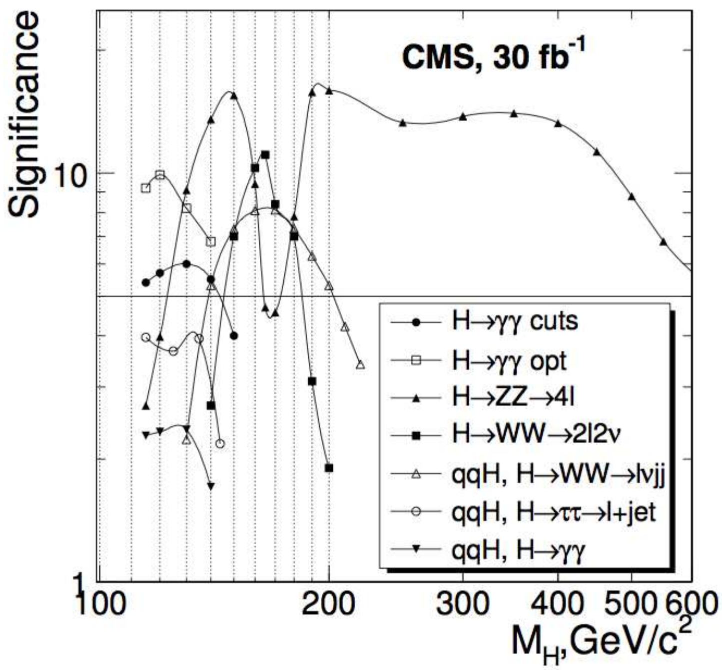

Fig. 31. The predicted sensitivity of the SM Higgs search by the CMS experiment.

16. C.S. Hill *et al.*, *Nucl. Instrum. Methods A* **530**, 1 (2004); A. Sill *et al.*, *Nucl. Instrum. and Methods A* **447**, 1 (2000); T. Affolder *et al.*, *Nucl. Instrum. Methods A* **453**, 84 (2000).
17. T. Affolder *et al.*, *Nucl. Instrum. Methods A* **526**, 249 (2004).
18. CDF uses a cylindrical coordinate system in which θ is the polar angle to the proton beam, ϕ is the azimuthal angle about the beam axis, and pseudorapidity is defined as $\eta = -\ln \tan(\theta/2)$. The transverse energy and transverse momentum are defined as $E_T = E \sin\theta$ and $p_T = p \sin\theta$, where E is energy measured in the calorimeter and p is momentum measured by the tracking system.
19. L. Balka *et al.*, *Nucl. Instrum. Methods A* **267**, 272 (1988); S. Bertolucci *et al.*, *Nucl. Instrum. Methods A* **267**, 301 (1988); M. Albrow *et al.*, *Nucl. Instrum. Methods A* **480**, 524 (2002).
20. CDF Collab. (A. Abulencia *et al.*), *J. Phys. G: Nucl. Part. Phys.* **34** 2457 (2007).
21. CDF Collab. (F. Abe *et al.*), *Phys. Rev. D* **45**, 1448 (1992).
22. A. Bhatti *et al.*, *Nucl. Instrum. and Methods A* **566**, 375 (2006).
23. CDF Collab. (D. Acosta *et al.*), *Phys. Rev. D* **71**, 052003 (2005).
24. CDF Collab. (A. Abulencia *et al.*), *Phys. Rev. D* **74**, 072006 (2006).
25. CDF Collab. (D. Acosta *et al.*), *Phys. Rev. Lett.* **95**, 051801 (2005).
26. CDF Collab., Search for Standard Model Higgs Boson Production in Association With a W Boson Using Matrix Element and Boosted Decision Tree Techniques With 2.7 fb^{-1} of CDF Data, in *CDF Note 9463*, (2008).
27. CDF Collab., Search for Standard Model Higgs Boson Production in Association with a W Boson Using Neural Networks With 2.7 fb^{-1} of CDF Data, in *CDF Note 9468*, (2008).

28. CDF Collab., A Search for $ZH \rightarrow l^+l^-b\bar{b}$ in 2.4 fb^{-1} using a Neural Network Discriminant, in *CDF Note 9475*, (2008).
29. J.Z. Efron, Ph.D. thesis, Ohio State University (2007), FERMILAB-THESIS-2007-20.
30. CDF Collab. (A. Abulencia *et al.*), *Phys. Rev. D* **74**, 032008 (2006).
31. M.L. Mangano, M. Moretti, F. Piccinini, R. Pittau and A.D. Polosa, ALPGEN, a generator for hard multiparton processes in hadronic collisions, in *JHEP* **07**, 001 (2003).
32. T. Sjostrand, P. Eden, C. Friberg, L. Lonnblad, G. Miu, S. Mrenna, and E. Norrbin, *Comput. Phys. Commun.* **135**, 238 (2001).
33. C. Peterson, T. Rognvaldsson and L. Lonnblad, JETNET 3.0: A versatile artificial neural network package, in *Comput. Phys. Commun.* **81**, 185 (1994).
34. CDF Collab., Search for the Standard Model Higgs Boson in the $\not{E}_T$ plus Jets Sample, in *CDF Note 9483*, (2008).
35. CDF Collab., A Search for the Standard Model Higgs Boson in the All-Hadronic Channel Using a Matrix Element Method, in *CDF Note 9366*, (2008).
36. CDF Collab., Search for the Standard Model Higgs Boson in the $H \rightarrow \tau^+\tau^-$ Channel at CDF Run II, Simultaneous Search for $WH/ZH/VBF/H$ Processes, in *CDF Note 9248*, (2008).
37. CDF Collab. (A. Abulencia *et al.*), *Phys. Rev. D* **75**, 092004 (2007).
38. CDF Collab., Search for $H \rightarrow WW^*$ Production at CDF Using 3.0 fb^{-1} of Data, in *CDF Note 9500*, (2008).
39. CDF Collab., Search for the WH Production Using High-p_T Isolated Like-Sign Dilepton Events in Run II with 1.9 fb^{-1}, in *CDF Note 7307*, (2008).
40. CDF Collab., Combined Upper Limit on Standard Model Higgs Boson Production for Summer 2008, in *CDF Note 9502*, (2008).
41. CDF Collab., Combined Upper Limit on Standard Model Higgs Boson Production, in *CDF Note 8941*, (2008).
42. The Tevatron New Phenomena and Higgs Working Group for the CDF and DØ Collaboration, Combined CDF and DØ Upper Limits on Standard Model Higgs-Boson Production with up to 2.4 fb^{-1} of data, in *hep-ex/0804.3423*.
43. The Tevatron New Phenomena and Higgs Working Group for the CDF and DØ Collaboration, Combined CDF and DØ Upper Limits on Standard Model Higgs-Boson Production at High Mass (155-200 GeV/c^2) with 3 fb^{-1} of data, in *hep-ex/0808.0534*.
44. CDF Collab., Search for Higgs Bosons Produced in Association with b-Quarks, in *CDF Note 9284*, (2008).
45. CDF Collab., Search for Neutral MSSM Higgs Bosons Decaying to Tau Pairs with 1.8 fb^{-1} of Data, in *CDF Note 9071*, (2007); CDF Collab. (A. Abulencia *et al.*), *Phys. Rev. Lett.* **96**, 011802 (2006).
46. CDF Collab., A Search for Charged Higgs in Lepton+Jets $t\bar{t}$ Events Using 2.2 fb^{-1} of CDF Data, in *CDF Note 9322*, (2008); CDF Collab. (A. Abulencia *et al.*), *Phys. Rev. Lett.* **96**, 042003 (2006).
47. T.P. Cheng and L.-F. Li, *Phys. Rev. D* **22**, 2860 (1980).
48. R.N. Mohapatra and J.C. Pati, *Phys. Rev. D* **11**, 566 (1975); G. Senjanovic and R.N. Mohapatra, *Phys. Rev. D* **12**, 1502 (1975); R.N. Mohapatra and G. Senjanovic, *Phys. Rev. D* **23**, 165 (1981).
49. C.S. Aulakh, A. Melfo and G. Senjanovic, *Phys. Rev. D* **57**, 4174 (1998); Z. Chacko and R.N. Mohapatra, *Phys. Rev. D* **58**, 015003 (1998).
50. CDF Collab. (D. Acosta *et al.*), *Phys. Rev. Lett.* **93**, 221802 (2004).
51. CDF Collab. (T. Aaltonen *et al.*), *Phys. Rev. Lett.* **101**, 121801 (2008).
52. CDF Collab. (D. Acosta *et al.*), *Phys. Rev. Lett.* **95**, 071801 (2005).
53. J. Konigsberg, CDF-2010, *Physics Advisory Committee Meeting, Nov. 2007*, Batavia,

Illinois, U.S.A. .
54. R. Roser, CDF through 2010, *Particle Physics Project Prioritization Panel Meeting, Feb. 2008*, Batavia, Illinois, U.S.A. .
55. CMS Collab., CMS Physics Technical Design Report Volume II : Physics Performance, in *CERN/LHC 2006-021*, (2006).
56. H.P. Nilles, Phys. Rep. **110** (1984) 1; H.E. Haber and G.L. Kane, Phys. Rep. **117**, 75 (1985).